Spectral Analysis of Absorption Features for Mapping Vegetation Cover and Microbial Communities in Yellowstone National Park Using AVIRIS Data

N

By Raymond F. Kokaly, Don G. Despain, Roger N. Clark, and K. Eric Livo

Chapter N *of*
Integrated Geoscience Studies in the Greater Yellowstone Area—Volcanic, Tectonic, and Hydrothermal Processes in the Yellowstone Geoecosystem

Edited by Lisa A. Morgan

Professional Paper 1717

U.S. Department of the Interior
U.S. Geological Survey

Contents

Figures

Tables

Spectral Analysis of Absorption Features for Mapping Vegetation Cover and Microbial Communities in Yellowstone National Park Using AVIRIS Data

By Raymond F. Kokaly,[1] Don G. Despain,[2] Roger N. Clark,[1] and K. Eric Livo[1]

Abstract

This report summarizes the application of imaging spectroscopy to the study of biotic components of Yellowstone National Park ecosystems. Maps of vegetation cover and hot-spring microorganisms were generated using spectral-feature analysis of data from the airborne visible and infrared imaging spectrometer (AVIRIS). AVIRIS data were calibrated to surface reflectance using a radiative-transfer model and a ground-calibration target. A spectral library of canopy-reflectance signatures was created by averaging pixels of reflectance data over known occurrences of 27 vegetation cover types in Yellowstone. Distributions of these vegetation types were determined by comparing absorption features of the vegetation in the spectral library with every pixel of the AVIRIS data using continuum removal and spectral analysis in the U.S. Geological Survey's Tetracorder expert system. Analysis of the chlorophyll- and leaf-water-absorption features (centered near 0.68, 0.98, and 1.20 μm, respectively) allowed accurate identification of vegetation cover types. Conifer cover types of lodgepole pine, whitebark pine, Douglas fir, and a mixed Engelmann spruce/subalpine fir class were spectrally identified and their distributions were mapped in AVIRIS images. Field-reflectance measurements revealed a distinct spectral signature of hot-spring microorganisms. These field measurements were added to the vegetation spectral library, and maps showing the distributions of microbial mats in the geyser basins of Yellowstone were produced.

Introduction

Yellowstone National Park (the Park) preserves and protects unique geologic features and biologic systems. This paper reports on efforts of the U.S. Geological Survey (USGS), in cooperation with the National Park Service, to apply imaging spectroscopy to map the distributions of vegetation species and microorganisms in Yellowstone ecosystems. The Park's ecosystems support many large mammals, whose populations and movements are directly and indirectly influenced by vegetation. In Yellowstone, the distributions of forest stands of whitebark pine affect the movements of grizzly bears (*Ursus arctos horribilis*) (Mattson and others, 1992). The large wildfires in 1988 increased interest in fire ecology and demonstrated how dramatically and rapidly the forests and the state of the ecosystem could change. Smaller organisms, the thermophilic bacteria of the hot springs, have received increasing scientific attention. Microorganisms in the unique hydrothermal environments of Yellowstone have been studied by biotechnology researchers because of their potential benefits for human health and their use in environmental remediation (Brock, 1994).

In comparison to multispectral broadband remote sensing, which only uses a few channels, imaging spectrometers measure the radiation upwelling from a surface in hundreds of contiguous, narrow bandwidth channels (Green and others, 1998). *Imaging spectroscopy* refers to analysis techniques that combine the spatial capability of an imaging system and the spectrometer's ability to resolve absorption features caused by the chemical bonds and affected by the physical structure of surface materials (Vane and others, 1993). In addition to imaging spectroscopy, other terms such as imaging spectrometry and hyperspectral, ultraspectral, and superspectral remote sensing have been applied to this type of remote sensing, to contrast it with traditional "multispectral" remote sensing (Clark, 1999). The advantage of spectroscopic over multispectral measurements is the ability to resolve absorption features and determine their specific wavelength positions and characteristic shapes. These absorption features are related to the material or materials causing them; thus, the materials present in a pixel of imaging-spectroscopy data can be identified (Mustard and Sunshine, 1999).

Approaches to mapping the distributions of materials in images have included the use of a reference set of spectra of known materials and "matching" algorithms (Clark and others, 2003; Van der Meer and Bakker, 1997; Adams and others, 1993; Boardman and Goetz, 1991; Clark and others,

[1]U.S. Geological Survey, Box 25046, MS 973, Denver Federal Center, Denver, CO 80225.

[2]U.S. Geological Survey, Biologic Resources Division, Box 173492, Montana State University, Bozeman, MT 59717.

1990; Mustard and Pieters, 1987). Those algorithms exploit the greater number of channels available and also directly take advantage of the spectrometer's power to resolve absorption features. Successful remote-sensing applications of spectral matching to identify Earth-surface materials have been advanced in the geological sciences, particularly with respect to mineral mapping (Swayze and others, 2000; King and others, 2000). These applications were highly successful in part because minerals have specific chemical compositions; thus, reflectance spectra of samples measured in the laboratory and spectra of outcrops on the landscape are comparable.

Vegetation cover has been mapped with imaging-spectroscopy data. In grasslands, the vegetation type and relative amounts of green and dry vegetation have been estimated with respect to soil background (Gamon and others, 1993). Roberts and others (1998) used airborne-spectrometer data, combined with spectral-mixture modeling, to map the distribution of different chaparral vegetation types in the Santa Monica Mountains of California. Airborne-imaging spectroscopy has been applied to forests of the Eastern United States in order to discriminate different forest types in an area of deciduous, mixed deciduous/conifer, and conifer cover (Martin and others, 1998). In those studies and spectral-mixture-analysis studies, a set of end-member spectra representing the vegetation cover, soils, and other surface materials of the area was matched with remotely sensed spectra. In those analyses, the full spectrum (all channels of the instrument) was used in the calculations. Other studies in vegetation analysis with spectroscopy suggested that only channels that correspond to the principal absorption features of vegetation (Kokaly, 2001; King and others, 2000; Kokaly and Clark, 1999; Kokaly and others, 1998) or that seem to offer the greatest separability between materials (Asner and Lobell, 2000) should be used.

In this paper, we report the use of imaging spectroscopy to map biologic materials in Yellowstone National Park using an analysis of spectral features. Vegetation spectra extracted from the AVIRIS data were assembled into a spectral-library database for Yellowstone vegetation. The USGS Tetracorder system (Clark and others, 2003; Clark and Swayze, 1995) was used to compare the spectral features of the AVIRIS pixels to the entries of the spectral library, using the chlorophyll- and leaf-water-absorption features. This approach to mapping vegetation utilized the absorption features caused by the biochemical composition of plants and affected by the architecture of vegetation canopies. This report first presents background information on the vegetation of Yellowstone and on past applications of remote sensing to the mapping of forest cover. Then, spectral-analysis techniques used to detect and map vegetation cover and hot-spring microorganisms are described. The spectral differences between vegetation cover types in Yellowstone National Park are presented and discussed. Finally, the resulting maps of vegetation cover and hot-spring microorganisms are presented, and their contributions to understanding hydrothermal systems and to examining the links between the distributions of plant species and large mammal populations are discussed.

Background

Yellowstone Vegetation

Most of the forests of Yellowstone National Park consist of five conifer species (Despain, 1990): lodgepole pine (*Pinus contorta*), whitebark pine (*Pinus albicaulis*), Douglas fir *(Pseudotsuga menziesii*), Engelmann spruce (*Picea engelmannii*), and subalpine fir (*Abies lasiocarpa*). The temperate forests at high altitudes in the Park receive large amounts of precipitation during the long, cold winter. According to Despain (1990), the mean duration of snow cover at 2,740-m altitude is about 271 days. At lower altitudes, in relatively drier valleys, grasslands and sagebrush steppe communities predominate.

The geology underlying the vegetation in Yellowstone influences the distribution of plants within the Park (Despain, 1990). In areas underlain by andesitic rocks, a higher nutrient content supports climax forests of mixed Engelmann spruce/subalpine fir. Douglas fir is present in moist areas, such as on north-facing slopes. Soils derived from rhyolite volcanic flows have relatively low nutrient content; in these areas, the dominant forest type is lodgepole pine. Thus, a strong geobotanical link is demonstrated between the species composition of conifer-forest stands and the availability of nutrients in soils derived from volcanic rocks.

As a result of fire history and soil conditions, the current dominant forest cover in Yellowstone is lodgepole pine. Despain (1990) delineated five cover-type categories for lodgepole pine based on forest structure and composition, fire characteristics, and age of the stand (LP0, LP1, LP2, LP3, and LP). The youngest age class, LP0, is young forest growth, commonly post-fire regrowth, with an age of 0 to 45 years. Since the large fires in 1988, LP0 has been a major cover type in the Park. LP1 forest stands range in age from approximately 45 to 150 years. These stands are small-diameter lodgepole with very sparse forest-floor vegetation. LP2 cover-type stands are closed canopy stands that still are dominated by lodgepole pine and range in age from 150 to 300 years. The understory is Engelmann spruce and subalpine fir seedlings and saplings. Depending on soil conditions, the final seral stage (older than 300 years) of lodgepole pine is either LP or LP3. Forest stands on rhyolite-derived or other dry soils are dominated by lodgepole pine, with some whitebark pine possibly growing in the overstory and understory (this cover type is designated LP). The LP3 cover type has an uneven canopy composed of a mixture of lodgepole pine, Engelmann spruce, subalpine fir, and whitebark pine. The LP3 understory consists of small and large spruce and fir seedlings and saplings.

Nonforest vegetation in Yellowstone National Park is divided into four major groups: grassland, sagebrush steppe, wet sedge and willow meadow, and alpine meadow. The distributions of these vegetation types are influenced by precipitation and soil characteristics, and, consequently, they

are strongly related to altitude. Big sagebrush grows in dry to moderately moist areas at middle and lower altitudes, such as in the Lamar River valley. Silver sage grows in wetter areas higher than 2,130 m, for example, in the Hayden and Pelican Valleys. Alpine meadows are present at altitudes higher than 3,050 m. Sedge marshes and other wetland vegetation thrive in areas of year-long standing water at various altitudes throughout the Park. Willows and sedges grow along streams and near seeps.

Reflectance Spectra of Plants

Spectroscopy can provide information about a substance by relating the interaction of electromagnetic radiation as a function of wavelength to its chemical composition and physical properties. All vegetation contains the same basic constituents: chlorophyll and other light-absorbing pigments, water, proteins, starches, waxes, and structural biochemical molecules such as lignin and cellulose (Elvidge, 1990). All of these components contribute to the reflectance spectra of vegetation. Figure 1 shows laboratory reflectance spectra of vegetation foliage in both the fresh state and after being dried in an oven for 24 hours. The wavelength regions in which the basic plant components have strong absorption features are indicated on this plot. Because of pigment absorptions, the visible region of green plants shows a maximum reflectance at approximately 0.55 μm and lower reflectance in the blue (0.45 μm) and red (0.68 μm).

Beyond visible wavelengths (longer than 0.70 μm), the spectra of fresh plants show a strong rise in reflectance. The region of high plant reflectance at the short-wavelength end of the near-infrared (0.75–1.30 μm) is called the near-infrared plateau (NIR-plateau). The high reflectance results from an increased amount of light scattering at cell-wall interfaces because of a change in the index of refraction,

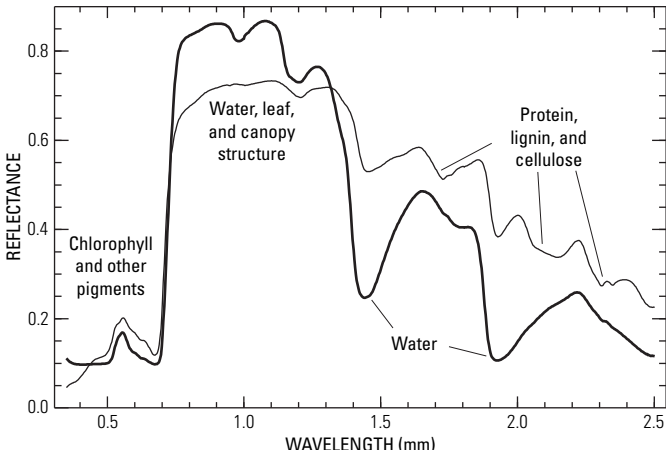

Figure 1. Laboratory reflectance spectra of an oak leaf in fresh (thick line) and dry (thin line) states. The causes of major plant absorption features are indicated. Reflectance is unitless.

the absence of pigment absorptions, and the weakening of overtone absorption of water in leaves at those wavelengths. Two absorption features centered near 0.98 and 1.20 μm are evident on the NIR-plateau. At 1.40 μm, a strong water-absorption feature reduces the reflectance. For fresh leaves, another, even stronger, water absorption is present at 1.90 μm. In dried vegetation, the water absorptions no longer conceal the absorption features at 1.73 μm, 2.10 μm, and 2.30 μm that are caused by organic bonds in plant biochemicals. Proteins, lignin, and cellulose all contribute to these features. C-H, N-H, and C-O bonds in the organic molecules have overtones and combinations that absorb in the near-infrared region of the spectrum (Peterson and Hubbard, 1992; Kokaly, 2001).

Remote Sensing of Vegetation in Yellowstone National Park

Remote sensing of vegetation is rooted in the interpretation of aerial photography. Photographs taken with airborne cameras have very high spatial resolution. By comparison of "textures," which includes the crown shape, density, and color of vegetation, different vegetation species are identified (Howard, 1991). Despain (1990) used aerial photography of Yellowstone National Park to construct a vegetation map. His map showed the distributions of the five major conifer species, the various age classes of lodgepole pine, and nonforest vegetation.

The development of digital sensors flown on satellites allowed vegetation mapping to be conducted on regional scales. These systems now are used routinely to map the distribution and quality of vegetation (Teillet and others, 1997; Huete and others, 1999). In particular, the Landsat MSS (multispectral scanner) and TM (thematic mapper) instruments, with 80- and 30-m resolution, respectively, have been applied widely to regional studies of vegetation. Jakubauskas (1996) used Landsat TM data to map the distribution of forest cover types in Yellowstone National Park. He demonstrated that lodgepole pine forest types had differing reflectance characteristics as a function of age.

Methods

AVIRIS Data Collection for Yellowstone National Park

For this study, the airborne visible and infrared imaging spectrometer (AVIRIS), operated by NASA's Jet Propulsion Laboratory, was used. AVIRIS collects data in 224 continuous channels of approximately 10-nanometer bandpass over the spectral-wavelength range of 0.35 to 2.50 μm (from visible light to near-infrared). In Yellowstone, for the mean altitude of 2,290 m, AVIRIS measured pixels with a nominal size of 17.5 m.

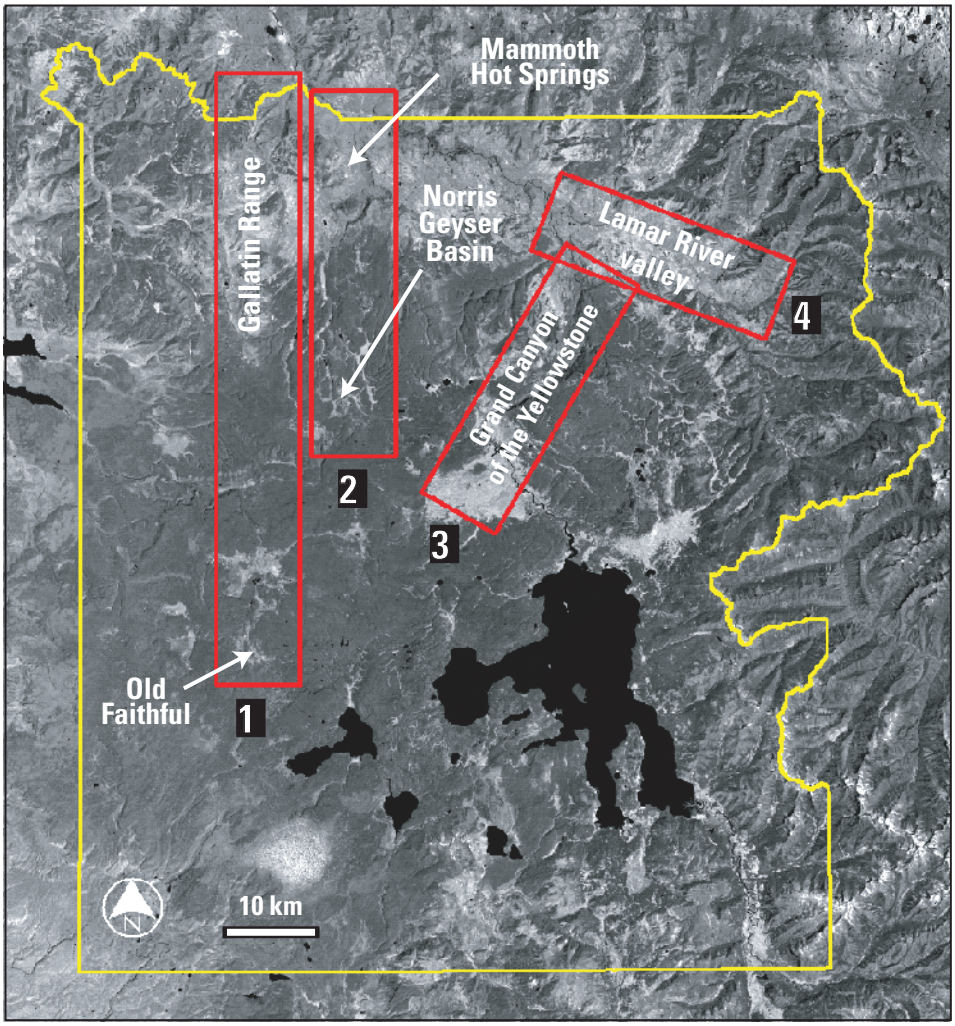

Figure 2. Coverage of AVIRIS data collected on August 7, 1996, over Yellowstone National Park (the Park boundary is indicated). The four flight lines, approximately 10 km wide, include: line 1—north from the Old Faithful area to the Gallatin Range; line 2—north from Norris Geyser Basin to Mammoth Hot Springs and Gardiner, Montana; line 3—Grand Canyon of the Yellowstone River and Mount Washburn; and line 4—Lamar River valley.

The cross-track pixel sampling at nadir was 15.4 m and along-track sampling was 17.5 m, given the aircraft ground speed of approximately 210 m/s. The sensor-swath width was approximately 10 km.

AVIRIS data were collected on August 7, 1996, in four flight lines that included the following areas: Upper and Lower Geyser Basins, Gallatin Mountain Range, Mammoth Hot Springs, Norris Geyser Basin, Grand Canyon of the Yellowstone River, and the Lamar River valley. Those areas were selected to target areas of primary geologic and biologic interest. The outlines of the AVIRIS flight lines are shown in figure 2.

AVIRIS Data Calibration

To convert AVIRIS data from radiance to reflectance, the data were corrected for the influence of several variables, including solar irradiance, atmospheric-gas absorptions, and atmospheric scattering. We employed a two-step procedure for this conversion, as described in Clark and others (2003) and Rockwell and others (2002). First, the atmospheric-removal algorithm (ATREM; Gao and others, 1993, 1997) was applied to the radiance data. This radiative-transfer model removed most of the atmospheric effects. Unfortunately, residual atmosphere absorptions remained in the data, including an overcorrection of the atmospheric-path radiance. An additive correction for path radiance was derived using ATREM reflectance of a vegetation-covered area in shadow (Clark and others, 2003). Next, field-reflectance measurements of a ground-calibration site were used to reduce the atmospheric residuals. A gravel-staging site near Norris Geyser Basin was used for calibration because it was fairly large and homogenous, and it did not contain materials with strong absorption features. On the day of the AVIRIS flight, reflectance measurements of the staging site were made with an analytical spectral device (ASD) full-range field spectrometer. The averaged field measurements were corrected for the small absorption features of the Spectralon (Labsphere, Inc., North Sutton, N.H.) reference-calibration standard. The field measurement was used with the averaged ATREM data over the calibration site to generate the multiplicative correction. The resulting reflectance data are termed radiative-transfer ground-calibrated (RTGC) reflectance data. Kokaly and others (2003) described the calibration procedure in detail.

Spectral-Feature Analysis and Mapping Methods

The approach to vegetation mapping in this study uses comparisons of the spectral features of known vegetation cover types to the spectral features in each pixel of remote-sensing data. The following sections present the critical parts of this approach: (1) techniques of spectral-feature analysis used to isolate and normalize absorption features in reflectance data, (2) the creation of a spectral library of vegetation cover in Yellowstone National Park, and (3) compilation of vegetation maps by applying a spectral-feature-fitting algorithm and expert-system rules in the USGS Tetracorder system to the AVIRIS data and the vegetation spectral library.

Spectral-Feature Analysis

To compare the shapes of the absorption features, this study used a method of normalization called continuum removal. The continuum is simply an estimate of the other absorptions present in the spectrum, not including the one of interest (Clark and Roush, 1984; Clark, 1999). The first step in continuum removal is selection of the continuum endpoints (λ_1 and λ_2), which may be established at the points of minimum absorption surrounding the absorption feature. Following the selection of endpoints, the continuum may be modeled using a linear, polynomial, or other mathematical function. In practice, linear segments can be used to approximate the continuum, offering the advantage of easy computation. However, a Gaussian analysis probably is more accurate for strong overlapping absorptions (for example, see Clark 1981; Sunshine and others, 1990; Sunshine and Pieters, 1993).

After the continuum line (R_L) is established, the continuum-removed spectrum (R_C) is calculated by *dividing* the original reflectance values (R_O) by the corresponding values of the continuum line for all the channels in the wavelength region (λ_1 to λ_2) of the absorption feature:

$$R_C(\lambda) = R_O(\lambda) / R_L(\lambda) \quad (1)$$

To illustrate application of continuum removal, the reflectance spectra of two conifers (shown in fig. 3*A*) are used. By applying linear-continuum removal, it is clear that the reflectance from Douglas fir has a deeper chlorophyll absorption than that of lodgepole pine (fig. 3*B*). The greater depth of the Douglas fir absorption feature is a result of stronger absorption by chlorophyll. At the leaf level, this possibly is caused by greater concentration of the pigment. For reflectance spectra of canopies, the depth of the chlorophyll absorption varies because of many factors including: (1) the concentration of chlorophyll in the understory and overstory, or both; (2) the effects of multiple scattering between canopy elements; and (3) changes in fractional cover of vegetation over the soil background. The depth (D) of the absorption feature at each channel is calculated by

$$D(\lambda) = 1 - R_C(\lambda) \quad (2)$$

The band center (λ_C) of the absorption feature is the wavelength position of the spectrometer channel with the maximum depth. The absorption depth at the band center, D_C, is referred to as the band depth. More complex determinations of the wavelength position of the absorption-band center, which are less instrument specific, are made by fitting of mathematical functions to the channels near the absorption center (see for example, Choquette and others, 1998).

Scaling of absorption features to the same band depth at the band center facilitates visual comparison of the shapes. From the reflectance spectra of the same absorption feature in different samples, the continuum-removed absorption features can be scaled to equal depth at the band center. An example of this is shown in figure 3*C*. The scaling reveals that, in addition to the greater band depth, the reflectance spectrum of Douglas fir has a wider chlorophyll-absorption feature compared to that of lodgepole pine. The spectral differences between these two conifers suggest that spectroscopic remote sensing can be used to distinguish conifer forest cover types based on subtle differences in their reflectance spectra.

Spectral Library for Yellowstone Vegetation

The major cover types in Yellowstone National Park were identified during a field survey. These cover types included all significant forest cover types, including lodgepole pine, whitebark pine, Douglas fir, and a mixed Engelmann spruce/subalpine fir category. Because lodgepole pine covers the greatest area in the Park and is the major colonizing species on recently disturbed ground, five classes of lodgepole pine were used. In addition, areas of nonforest vegetation were identified. These nonforest types included sagebrush, willow, Idaho fescue grasslands, lush sedge habitats, and wetland areas.

To establish spectral signatures of these vegetation types, pixels in the AVIRIS data covering the vegetation types were averaged to generate representative spectra. Thirty-seven areas were identified in the AVIRIS data. More than one area was used for some vegetation cover classes. Table 1 lists the forest cover types (boldface indicates entries for which the spectra are used in figures in this paper). Table 2 lists the nonforest cover types and the names used to label the subsequent plots. These averaged AVIRIS spectra for the vegetation cover types in tables 1 and 2 constitute the reference spectral library used by the Tetracorder system in this study.

In addition to vegetation cover, spectra of hot-spring microorganisms were included in the reference library. During field surveys, we measured the reflectance spectra of hot-spring bacteria and algae. The spectral shapes were

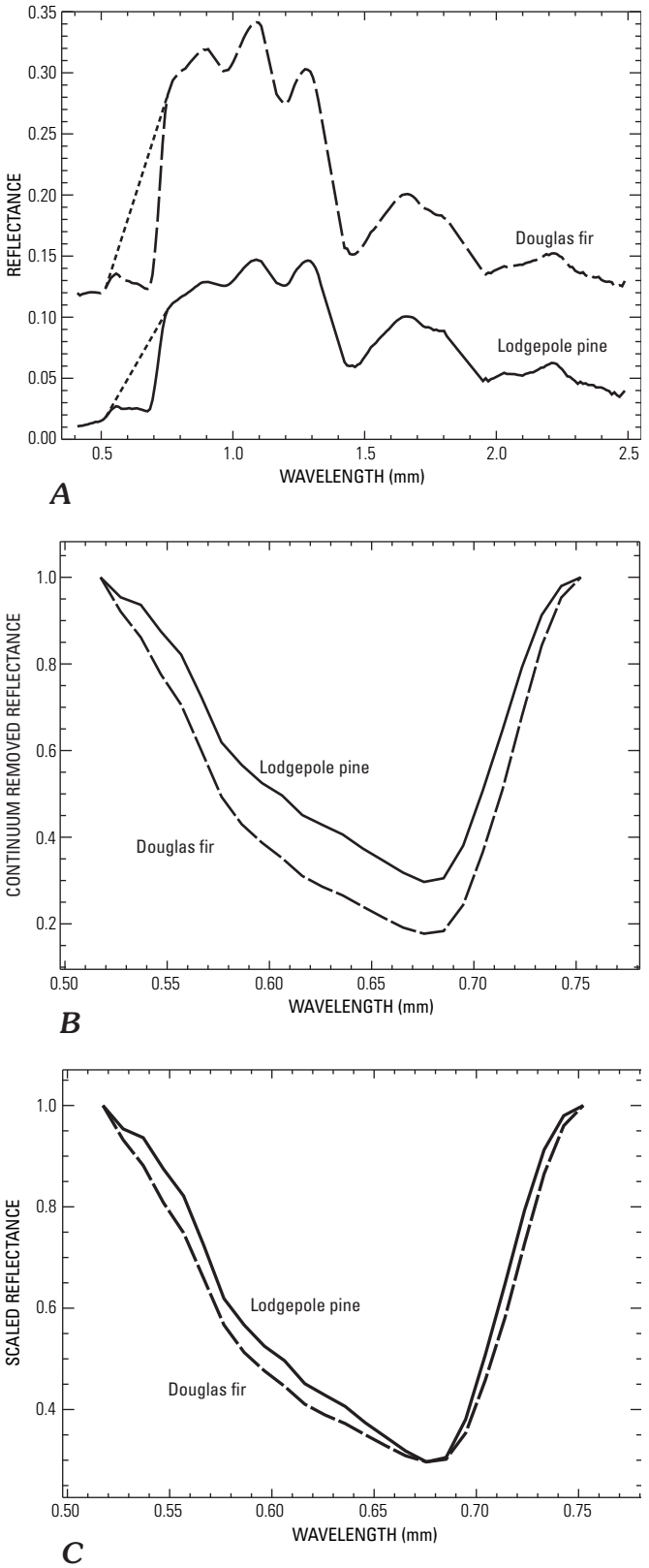

Figure 3. AVIRIS radiative-transfer ground-calibrated reflectance spectra of Douglas fir and lodgepole pine with associated continuum lines. *A*, Reflectance spectra are offset by 0.1 in reflectance. *B,* Continuum-removed chlorophyll absorption-feature spectra. *C,* Scaled chlorophyll absorption features.

unique, compared to those of vegetation. Figure 4 shows a spectrum of a hot-spring-bacteria mat that contains a thick surface layer of the thermophilic bacterium *Synechococcus* sp. Compared to features of vegetation, the chlorophyll absorption is narrow and the water absorptions are very strong. All spectra used in this study are published in Clark and others (2003) and are available online at http://speclab.cr.usgs.gov/spectral-lib.html.

Although the atmospheric correction and ground calibration of AVIRIS data were performed, some channels were deleted from the mapping analysis (and the plotted spectra in this paper) because of residual atmospheric effects. The channels in which detector overlaps are present were also excluded from analyses. These excluded channels are listed in table 3.

The USGS Tetracorder System

Tetracorder is an expert system. It compares the absorption features present in each pixel of AVIRIS data to the characteristic absorption features of materials in a spectral library (Clark and others, 1990, 1991; Clark, Swayze, and others, 1993; Clark and Swayze, 1995; Clark and others, 2003). Tetracorder uses continuum removal to isolate specific absorptions and to remove the effects of changing slopes and overall reflectance levels. It compares the shapes of absorption features in the AVIRIS data with those in each reference sample of the library. A modified least-squares-fitting algorithm numerically determines the best match between the spectral features in a pixel of AVIRIS data and those in the entries of the spectral library. The Tetracorder system can make further refinements to the selection of the closest match with a set of expert-system rules, including definition of threshold values, continuum-slope constraints, and other methods (see detailed explanation in Clark and others, 2003).

Tetracorder uses user-specified continuum endpoints, linear-continuum removal, and a modified, linear, least-squares-fitting algorithm to scale the absorption feature of a library-reference spectrum to match the feature in an AVIRIS pixel (for details see Clark and others, 2003). The least-squares fitting uses all the channels in the feature to adjust the depth of the reference spectrum to the depth of the feature in the spectrum of the unknown material in the AVIRIS pixel. The depth of the feature in the unknown spectrum is calculated as the band depth of the library-reference spectrum that was scaled to it, in order to avoid calculations using the noisier AVIRIS spectrum. In Tetracorder, the correlation coefficient (r) resulting from the least-squares fitting is used to assess the *goodness of fit* between the continuum-removed spectral features of the library and the unknown spectra.

For the comparison of the entries of a spectral library to the spectrum of an AVIRIS pixel using only a single absorption feature, the fit values calculated between the library entries and the pixel are compared and the entry

Table 1. Spectral library entries of forest cover types.

[Bold type indicate entries used in figures of reflectance spectra in this paper]

Forest cover type	Training site location	Number of pixels, averaged
Douglas fir	Mammoth (line 2)	114
Douglas fir	Gallatin Range (line 1)	84
Douglas fir	Lamar Valley (line 4)	207
Whitebark pine	Mt Washburn (line 3)	34
Whitebark pine	Gallatin Range (line 1)	105
Engelmann spruce/subalpine fir	Mt Washburn (line 3)	18
Engelmann spruce/subalpine fir	Mt Washburn (line 3)	20
Engelmann spruce/subalpine fir	Gallatin Range (line 1)	257
Engelmann spruce/subalpine fir	Gallatin Range (line 1)	99
Engelmann spruce/subalpine fir	Gallatin Range (line 1)	126
Aspen	Lamar Valley (line 4)	15
Lodgepole pine age class 0—moderate regrowth	Mammoth (line 2)	371
Lodgepole pine age class 0—vigorous regrowth	Mammoth (line 2)	56
Lodgepole pine age class 1	Mt Washburn (line 3)	72
Lodgepole pine age class 1	Mammoth (line 2)	144
Lodgepole pine age class 1	Norris (line 2)	135
Lodgepole pine age class 1	Mammoth (line 2)	129
Lodgepole pine age class 2	Mammoth (line 2)	30
Lodgepole pine age class 2	Mammoth (line 2)	128
Lodgepole pine age class 3	Mt Washburn (line 3)	132
Lodgepole pine age class 3	Mt Washburn (line 3)	52
Lodgepole climax age class	Norris (line 2)	148
Lodgepole pine meadow mix	Mt Washburn (line 3)	153

with highest fit value (r) is selected as the best match. In Tetracorder, multiple absorption features in a single material (that is, a library entry) are used with a list of user-specified constraints to select the best match (Clark and others, 2003). A standard constraint in the applications of Tetracorder is the definition of a minimum continuum-threshold level. Deeply shadowed pixels have low reflectance (for example, pixels along the north-facing slope of a canyon). Such pixels have a low signal-to-noise ratio, making it difficult to discern absorption features through the high noise level. In Tetracorder, a minimum threshold level of 4-percent reflectance was set arbitrarily for the midpoint of the continuum for all entries in the Yellowstone vegetation spectral library. For pixels with a continuum-reflectance level below this threshold, Tetracorder did not attempt to determine the vegetation cover type.

In this application of Tetracorder to the mapping of vegetation in Yellowstone National Park, we selected three absorption features to use in the comparison of AVIRIS data to the spectral library. The absorptions used were the 0.68-μm chlorophyll-absorption feature, the 0.98-μm leaf-water, and the 1.20-μm leaf-water absorptions. Table 4 shows the continuum endpoints used by the Tetracorder analysis for the three features. A range of wavelengths was selected as the endpoints of the continuum. In the computation of the continuum line, the AVIRIS channels within these ranges were averaged to reduce the effect of noise in the computations (Clark and others, 2003).

In this study, the fit values for each of the three absorption features, the chlorophyll and two water absorptions, were weighted by approximately 0.70, 0.15, and 0.15, respectively, and summed. These weights gave more emphasis to the stronger chlorophyll absorption. Thus, for a pixel in the AVIRIS data, the Tetracorder system calculated a total weighted-fit value for each entry in the spectral library. Subsequently, the "best match" of the AVIRIS pixel to the spectral library was selected as the highest weighted-fit value. For each entry in the spectral library, a raster image was produced by assigning the fit value to the pixels for which the cover type was selected as the best match (all other pixels were set to zero). Thus, for an entry in the spectral library, its raster "fit" image shows the distribution of pixels that have the closest spectral appearance to the entry compared to the other entries in the library. The pixel values are an indication of the closeness of the match between the pixel spectrum and the library spectrum. Thus, the range in values of the pixels is a measure of the degree of confidence in the match, and the image can be processed with simple contrast stretching to represent either the full range of fit values or only the relatively high fit values. By selecting different colors for each cover type, fit images were combined to produce thematic maps of conifer, non-forest, and microbial cover.

Table 2. Spectral library entries of nonforest cover types.

Cover type category	Plot name	Cover type	Major vegetation species occurring in cover type	Training site area	Number of pixels
Sagebrush shrubland	sage1	Sagebrush and grass	*Artemisia tridentata, Festuca idahoensis*	Mammoth (line 2)	216
Sagebrush shrubland	sage2	Sagebrush and grass	*Artemisia tridentata, Festuca idahoensis*	Mammoth (line 2)	81
Sagebrush steppe	sage/fescue1	Mixed sage and grass	*Artemisia tridentata, Festuca idahoensis, Geranium viscosissimum*	Lamar Valley (line 4)	129
Sagebrush steppe	sage/fescue2	Mixed sage and grass on north-facing slope	*Artemisia tridentata, Festuca idahoensis, Geranium viscosissimum*	Lamar Valley (line 4)	51
Grassland	fescue/wheatgrass1	Mixed Idaho fescue and bearded wheatgrass—wet phase	*Festuca idahoensis, Agropyron caninum, Geranium viscosissimum*	Lamar Valley (line 4)	62
Grassland	fescue/wheatgrass2	Mixed Idaho fescue and bearded wheatgrass—dry phase	*Festuca idahoensis, Agropyron caninum*	Lamar Valley (line 4)	56
Grassland	fescue/wheatgrass3	Mixed Idaho fescue and bluebunch wheatgrass	*Festuca idahoensis*, *Agropyron spicatum*	Lamar Valley (line 4)	78
Grassland	fescue/needlegrass	Mixed Idaho fescue and Richardson's needlegrass	*Festuca idahoensis, Stipa richardsonii*	Lamar Valley (line 4)	510
Grassland	bromus	Smooth brome	*Bromus inermis*	Lamar Valley (line 4)	65
Wet nonforest	willow/sedge	Willow and sedge	*Salix* sp., *Carex* sp.	Norris (line 2)	39
Wet nonforest	willow	Willow	*Salix* sp.	Norris (line 2)	30
Wet nonforest	sedge	Sedge	*Carex* sp.	Mammoth (line 2)	183
Wet nonforest	cattail	Cattails	*Typha* sp.	Old Faithful (line 1)	18
Wet nonforest	wetland1	Mixed wetland	Mixed wetland vegetation	Old Faithful (line 1)	11
Wet nonforest	wetland2	Mixed wetland	Mixed wetland vegetation	Norris (line 2)	53

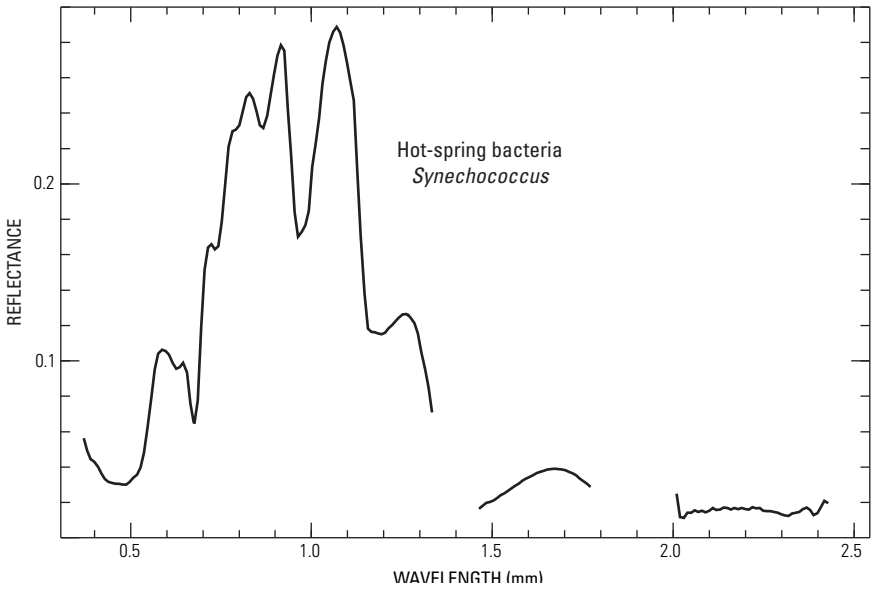

Figure 4. Field-reflectance spectrum of a Yellowstone hot-spring bacterial mat (primary organism is *Synechococcus* sp.).

Table 3. Channels of 1996 AVIRIS data not used in spectral analysis.

[N/A, not applicable]

Deleted channels	Wavelength region	Reason for deletion
1–4	< 0.40 μm	Decreasing signal from ozone absorption and an imprecise correction for atmospheric scattering
32–33	N/A	Overlap in detectors
43	0.71 μm	Oxygen absorption
59–62	centered at 0.98 μm	Atmospheric water vapor
81–84	centered at 1.20 μm	Atmospheric water vapor
95–97	N/A	Overlap in detectors
106–113	centered at 1.40 μm	Atmospheric water vapor
154–167	centered at 1.90 μm	Atmospheric water vapor
173–175	centered at 2.00 μm	Atmospheric carbon dioxide
223–224	> 2.49 μm	AVIRIS instrument performance degrades

Results and Discussion

In this study, vegetation mapping in Yellowstone National Park is focused on a comparison of the spectral features in each pixel of remote-sensing data to the spectral features of known vegetation cover types. The results are reported in the following two sections. First, the reflectance spectra of the vegetation cover types in Yellowstone are presented and the differences in absorption strengths are discussed. This discussion aids in interpretations of the vegetation maps, which are given in the final section.

Comparison of Spectra for Vegetation Cover Types

This section presents the reflectance spectra and continuum-removed absorption features of the vegetation cover types in Yellowstone National Park. For clarity, in the plots of spectra, only one representative spectrum from the spectral library of forest cover types, listed in table 1, is presented.

Reflectance Spectra

Reflectance spectra of the forest cover types are shown in figure 5*A*. In general, the forest cover types are designated by the dominant species: whitebark pine (WB), lodgepole pine (LP), Douglas fir (DF), and mixed Engelmann spruce/subalpine fir forest (SF). In Yellowstone, lodgepole pine covers the largest area in the Park and is the major colonizing species on recently disturbed ground; as a result, Despain (1990) delineated several age classes of lodgepole pine. Representative spectra of the lodgepole age classes, from the entries of forest cover types in the spectral library listed in table 1, are shown in figure 5*B*.

The nonforest vegetation cover types listed in table 2 were divided into three groups. The first group, the "wet" vegetation, is the relatively lush nonforest vegetation that contains a significant amount of chlorophyll and water in leaves. The second group, "grassland," contains vegetation cover types dominated by grass species. The third group, "sagebrush steppe," contains cover types with a significant amount of sagebrush in addition to grasses. The spectra of wet, grassland, and sagebrush steppe nonforest cover types are shown in figures 5*C* to 5*E*, respectively.

In general, the conifer-reflectance spectra in figure 5*A* have a low level of reflectance in the visible spectrum (less than 5 percent from the blue to red portion of the visible spectrum) and a maximum reflectance level of 15–24 percent at 1.1 μm in the near-infrared (NIR) plateau. The reflectance spectra of lodgepole age classes in figure 5*B* show a change in the NIR plateau in young to old stands. The spectrum of the LP0 age class, consisting of young lodgepole pine seedlings, shows the NIR plateau region to have weak leaf-water absorptions that are superposed on a generally positive slope. In contrast, the LP3 stand has strong leaf-water absorption features. The LP3 lodgepole stand has a broken overstory that is beginning to be replaced by a mixed spruce/fir overstory (Despain, 1990). As a result, the ragged canopies of LP3 have gaps in the overstory. The increased water absorption possibly arises from multiscattering of incident light in this variable-height canopy or from higher water content in the understory vegetation, or both.

The wet-nonforest cover types (willows and sedge marshes) have much higher reflectance in the NIR plateau (see fig. 5*C*), compared to the forest cover (fig. 5*A*). These cover types have reflectance from 30–50 percent at 1.1 μm. The leading edge (0.75–0.90 μm) of the NIR plateau shows some variation in slope, from a steep slope for the sedge spectrum to a nearly zero slope for the wetland1 spectrum (fig. 5*C*). The reflectance spectra of the grassland cover types in figure 5*D* show a range in spectral features. The variations are dependent on the moisture regimes in which the different cover types grow. Fescue/wheatgrass1 is in a moisture-rich area. This is reflected in the strong chlorophyll- and water-absorption features in its spectrum. In contrast, fescue/wheatgrass2, a drier phase of the fescue/wheatgrass1, shows the water features to be weaker, and the 2.10- and 2.30-μm absorption features are revealed.

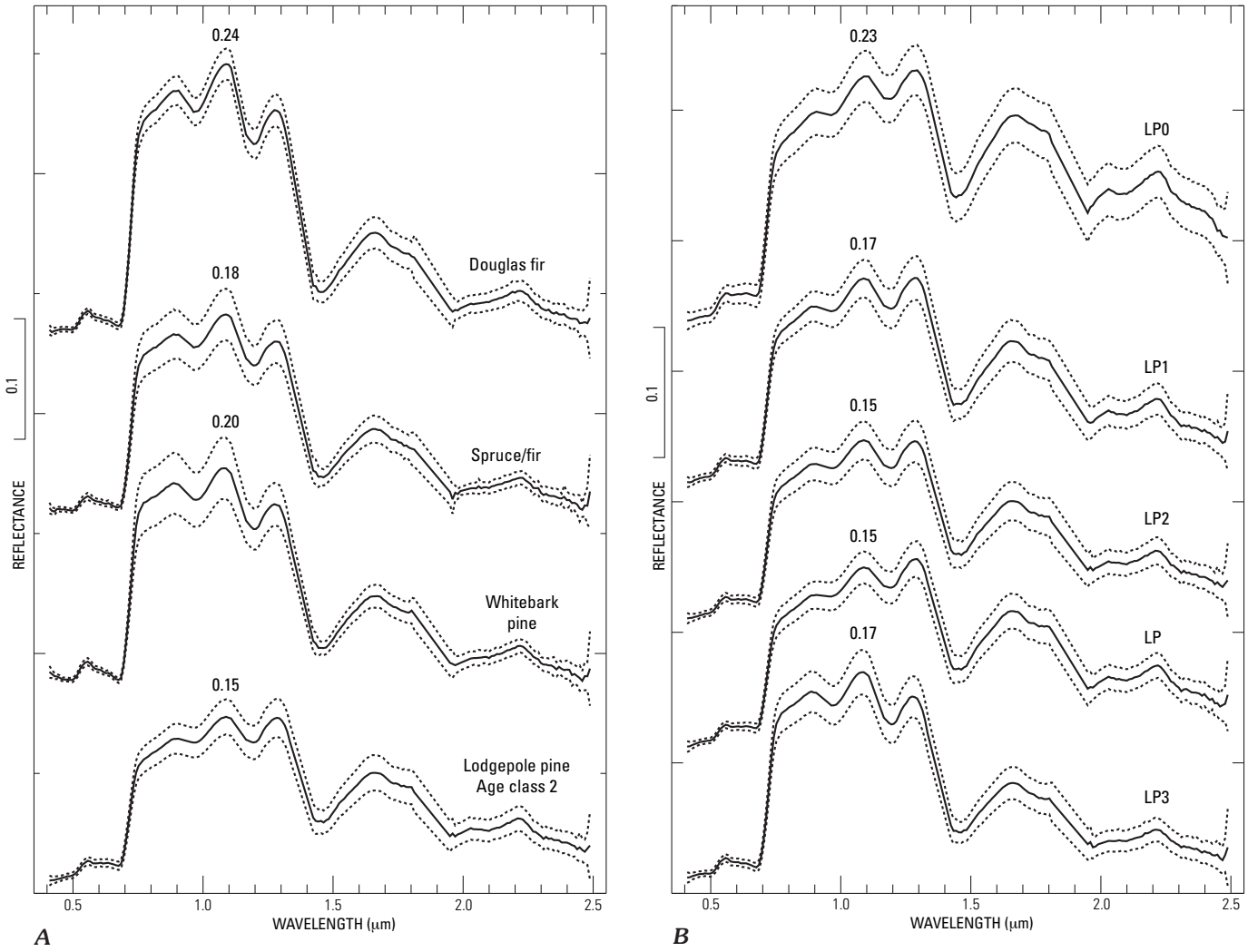

Figure 5. Representative AVIRIS radiative-transfer ground-calibrated reflectance spectra for Yellowstone vegetation (reflectance values at 1.1 μm are given in the figures). *A,* Conifer cover types; spectra are plotted at fixed intervals of 0.1 but offset by 0.15. *B,* Lodgepole pine age classes; spectra are plotted at fixed intervals of 0.1 but offset by 0.10.

The reflectance spectra of sagebrush steppe cover types (fig. 5*E*) differ greatly from those of forest and lush vegetation. These plants grow in sparse groups, and they had low water content at the time of the overflight (August 1996). Thus, the reflectance spectra of sagebrush steppe cover types show weaker absorption because of water. That weaker absorption reveals the longer wavelength absorptions at 2.10 and 2.30 μm that arise from leaf biochemical constituents (primarily lignin and cellulose). In addition to weaker water absorption, sagebrush leaves are covered by fine hairs that are composed mainly of cellulose; the hairs also will increase the longer wavelength absorption features at 2.10 and 2.30 μm. Furthermore, the spectra of the areas dominated by sagebrush (sage1 and sage2) show weak absorption at the 0.68-μm chlorophyll position because sagebrush plants have relatively low chlorophyll content and most grasses in these areas were senescent at the time of the AVIRIS overflight.

Continuum-Removed Vegetation-Spectral Features

The continuum-removed spectra for the chlorophyll-absorption feature are shown in figures 6*A* to 6*E* for the forest and lodgepole and nonforest wet, grassland, and sagebrush steppe cover types, respectively. Calculated band depths and band centers are given in table 5. For the forest-vegetation spectra shown in figure 6*A*, the pines show weaker absorption strengths, with lodgepole pine having the weakest chlorophyll absorption. Douglas fir has the strongest absorption feature. In figure 6*B*, the age classes of lodgepole pine show increasing band depth from the youngest class, LP0, to LP1, to LP2, and finally, to LP3.

The depth of chlorophyll absorption in these remotely sensed canopy spectra is due to both the concentration of chlorophyll in the leaves of the vegetation and the percent

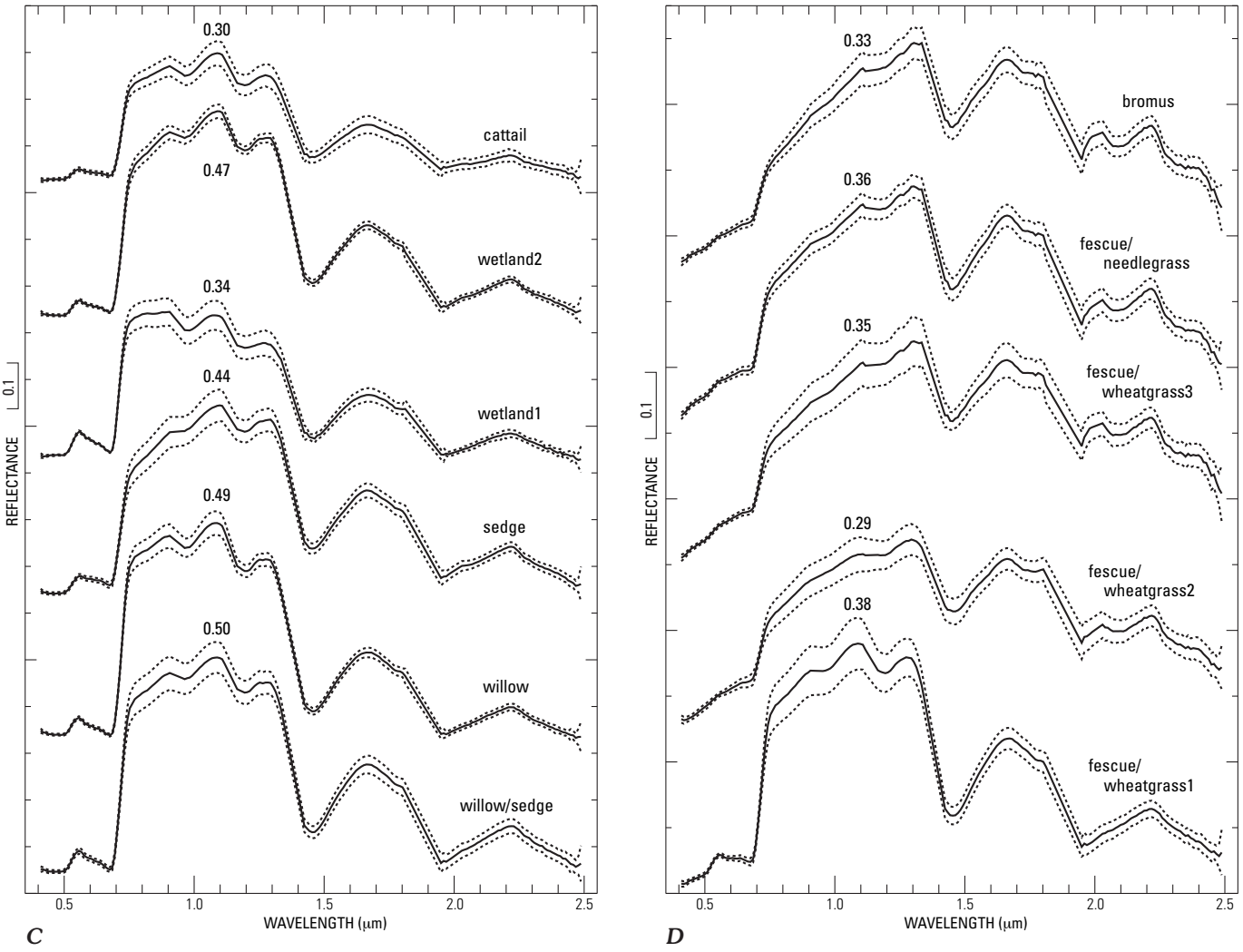

Figure 5 (continued). *C,* Lush nonforest vegetation; spectra are plotted at fixed intervals of 0.1 but offset by 0.25. *D,* Grassland cover types; spectra are plotted at fixed intervals of 0.1 but offset by 0.22.

cover of the vegetation over the background rocks and soils. Multiple scattering effects possibly affect the apparent strength of the chlorophyll absorption. A variable height canopy in LP3 possibly enhances multiple scattering between the overstory mature lodgepole pine and younger subalpine fir and Engelmann spruce in the understory, leading to a stronger absorption feature. The LP1, LP2, and LP age classes all show similar shapes of the chlorophyll absorption. Because of similarities of LP1, LP2, and LP spectra, these age classes of lodgepole pine are difficult to distinguish from one another spectrally, based only on the chlorophyll absorption.

Figure 6*C* shows the continuum-removed chlorophyll-absorption features for the areas of lush nonforest vegetation. In general, all of these features are stronger, in comparison to the other cover types (see the band depths in table 5). Within this group there is considerable variation in the shapes of the feature. This likely is caused by relative differences in concentrations of chlorophyll a and b, carotenes, and other accessory pigments among the cover types. At the time of the flight on August 7, 1996, the leaves of the nonforest plants in Yellowstone National Park were in various stages of senescence.

Figure 6*D* shows that, with the exception of fescue/wheatgrass1, all grassland areas contained low amounts of chlorophyll, as indicated by the shallow absorption feature. The spectra from these sites varied in the shape of the chlorophyll feature, and they are distinct from those of other cover types. The fescue/wheatgrass1 site contains a wet phase of the Idaho fescue/bearded wheatgrass grassland, and the stronger chlorophyll feature is consistent with this site retaining its chlorophyll later in the season because of available water, in comparison to the other grasslands. Figure 6*E* shows the chlorophyll absorption of the sagebrush areas. The mixed sage/grassland sites (sage/fescue1 and sage/fescue2) show more abundant chlorophyll in the vegetation, probably owing to a higher concentration of chlorophyll in the leaves as well as a higher percentage of total plant cover compared to the sage shrub lands (sage1 and sage2).

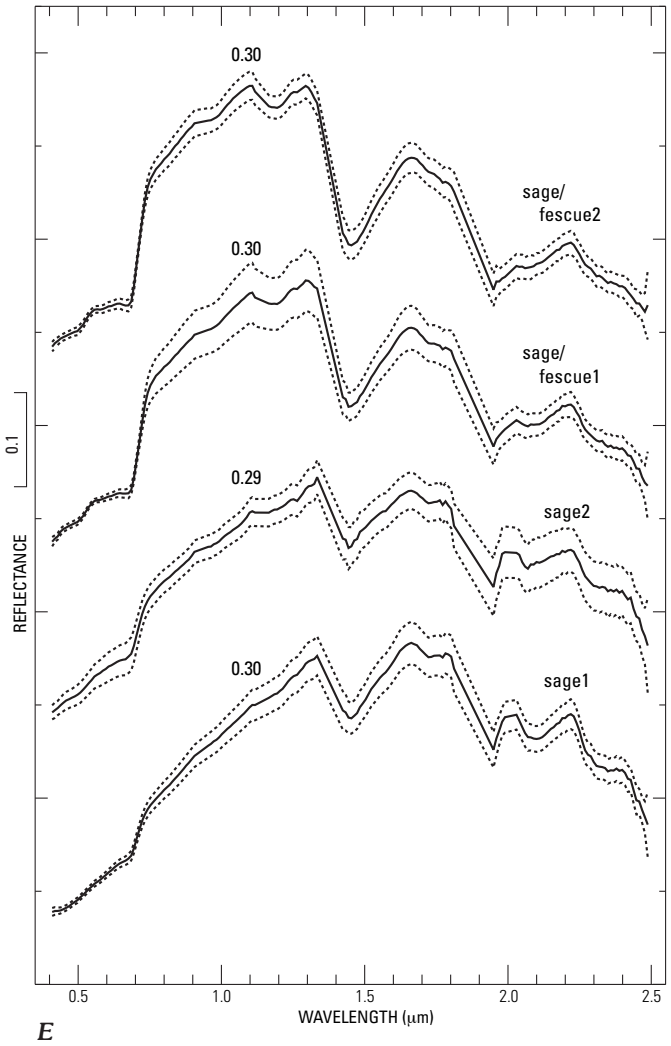

Figure 5 (continued). *E,* Sagebrush steppes; spectra are plotted at fixed intervals of 0.1 but offset by 0.20.

The continuum-removed 0.98-μm water-absorption features for the different forest areas are shown in figure 7*A*. Table 6 shows the band-depth and band-center positions of this absorption feature. In contrast to the chlorophyll-absorption feature, this feature shows that whitebark pine forest has stronger absorption than mixed Engelmann spruce/subalpine fir forest. Figure 7*B* shows that the LP1- and LP2- absorption features are extremely similar. The LP3 age class has the greatest water-absorption strength (band depth = 0.1074), at 0.98 μm, and LP0 has the weakest, at a band depth of 0.0601. The LP class has a weaker absorption than LP1 or LP2, but the overall shapes of the features are similar.

Figure 7*C* shows the 0.98-μm absorption feature owing to leaf water in the lush nonforest-vegetation types. The most distinguishing element of the shapes of these features, compared to other cover types, is the broad, flat bottoms of the features. The features here are flat from approximately 0.962 to 0.982 μm. In contrast, the forest-vegetation spectra show a narrow feature with a distinct band minimum at 0.982 μm (figs. 7*A* and 7*B*). Figure 7*D* shows that the 0.98-μm water-absorption features are weak for the grassland cover types, again with the exception of the fescue/wheatgrass1 site. The same features in the sagebrush sites are also weak, with depths of 3.5 percent or less (see fig. 7*E* and table 6). The absorption features for the sage shrub lands (sage and sage2) are extremely weak (<2 percent band depth). As a result, noise affects the shape of the absorption feature.

For the forest and lodgepole cover types, the shapes and band depths show similar trends in the 1.20-μm water-absorption feature as those for the 0.98-μm water-absorption feature (see Kokaly and others, 2003). Again, the wetland cover types have water absorption at 1.20 μm, with broad flat bottoms like those observed at 0.98 μm. Similar band depths and band-shape trends are present for the 1.20-μm water-absorption feature, when compared to the trends observed in the 0.98-μm water-absorption features for the grassland and sagebrush steppe cover types.

Maps of Vegetation and Microorganisms in Yellowstone National Park Derived from AVIRIS Data

Forest Cover

Using the results of the USGS Tetracorder system applied to the calibrated AVIRIS data and the vegetation spectral library, forest cover maps were produced that revealed distributions of conifer stands for areas of the Park covered by AVIRIS data. In this report, we focus on two specific areas of the Park for discussion: Mammoth Hot Springs and Mount Washburn. The map of forest cover for the Mammoth Hot Springs area of Yellowstone National Park is presented in figure 8. In this figure, the colored pixels representing the different forest cover types are overlaid on a gray-scale background image (the pixels in this figure that do not have mature forest cover are depicted in gray-scale tones).

The image for the area around Mammoth Hot Springs (fig. 8) shows that the forest cover is predominately lodgepole pine of various age classes (LP and LP1 to LP3). The fires of 1988 reduced much of the mature lodgepole forests in the southern half of the image in fig. 8. In the northern part of the scene, near Mammoth Hot Springs, large stands of Douglas fir (DF) are mapped. These stands also were indicated in aerial-photograph interpretations (Despain, 1990). This part of the scene was subject to much field verification, and agreement between both types of remote-sensing analysis and the field survey was good.

In another area of the scene, in the vicinity of Mount Everts, there was disagreement between the AVIRIS and aerial-photograph maps. The Tetracorder analysis of the AVIRIS data identified many pixels as either mixed Engelmann spruce/subalpine fir

Figure 6. Continuum-removed 0.68-μm chlorophyll-absorption spectra. *A,* Conifer cover types. *B,* Lodgepole pine age classes. *C,* Lush nonforest vegetation. *D,* Grassland cover types. *E,* Sagebrush steppes.

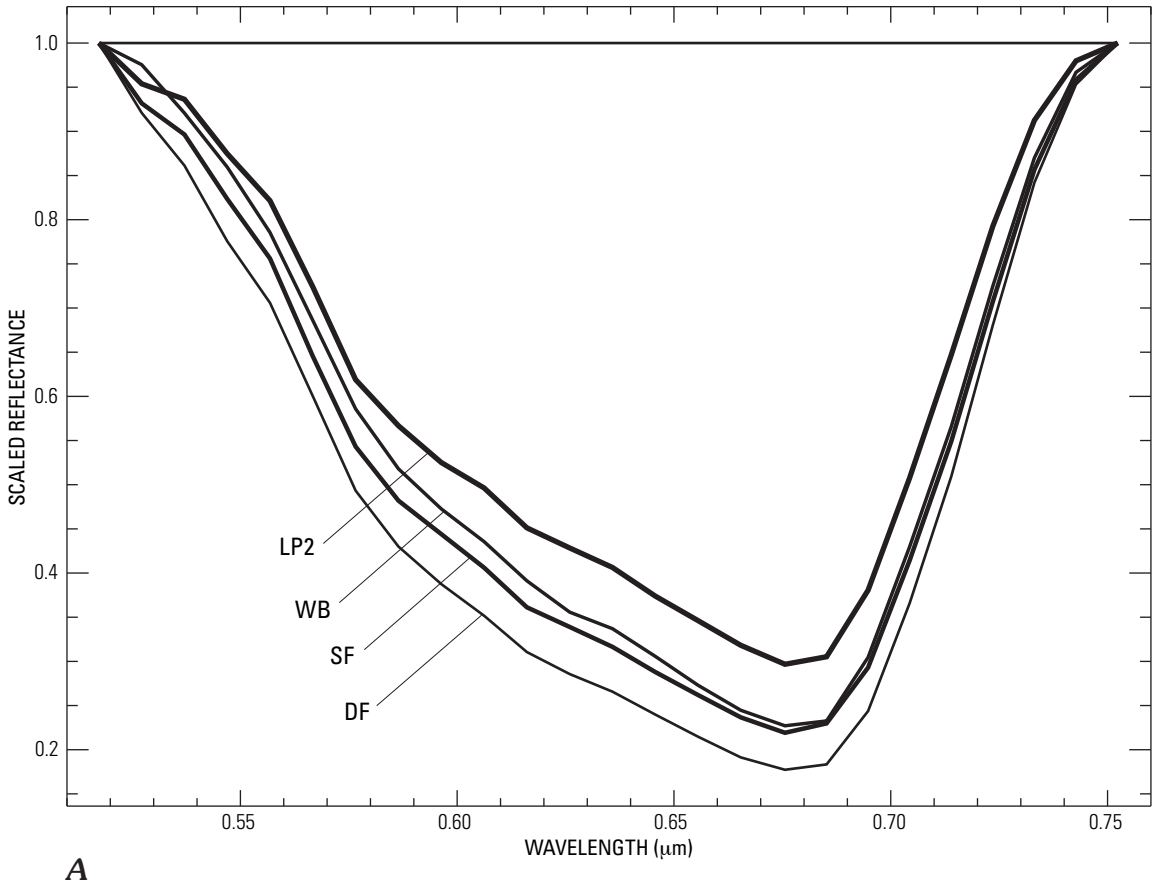
1.0
0.8
0.6
0.4
0.2
SCALED REFLECTANCE
LP2
WB
SF
DF
0.55
0.60
0.65
0.70
0.75
WAVELENGTH (μm)

A

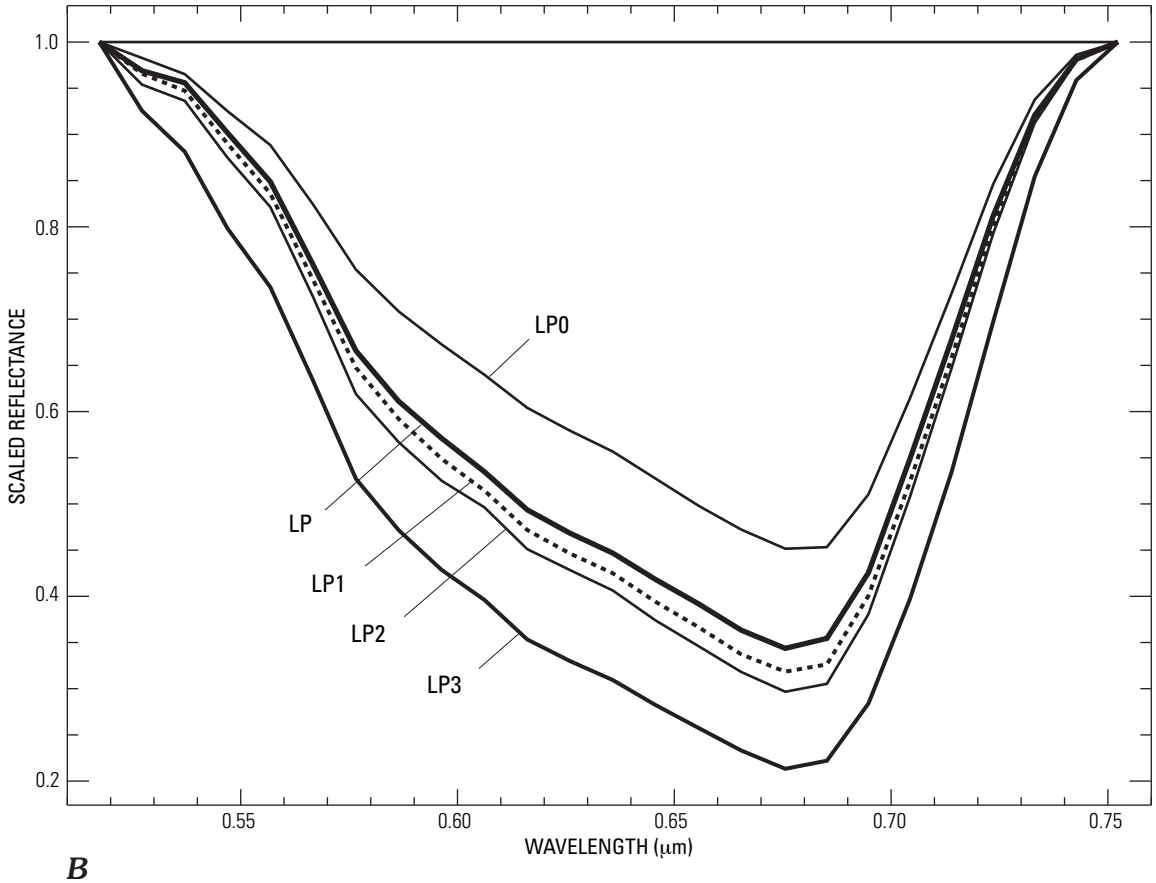
1.0
0.8
0.6
0.4
0.2
SCALED REFLECTANCE
LP0
LP
LP1
LP2
LP3
0.55
0.60
0.65
0.70
0.75
WAVELENGTH (μm)

B

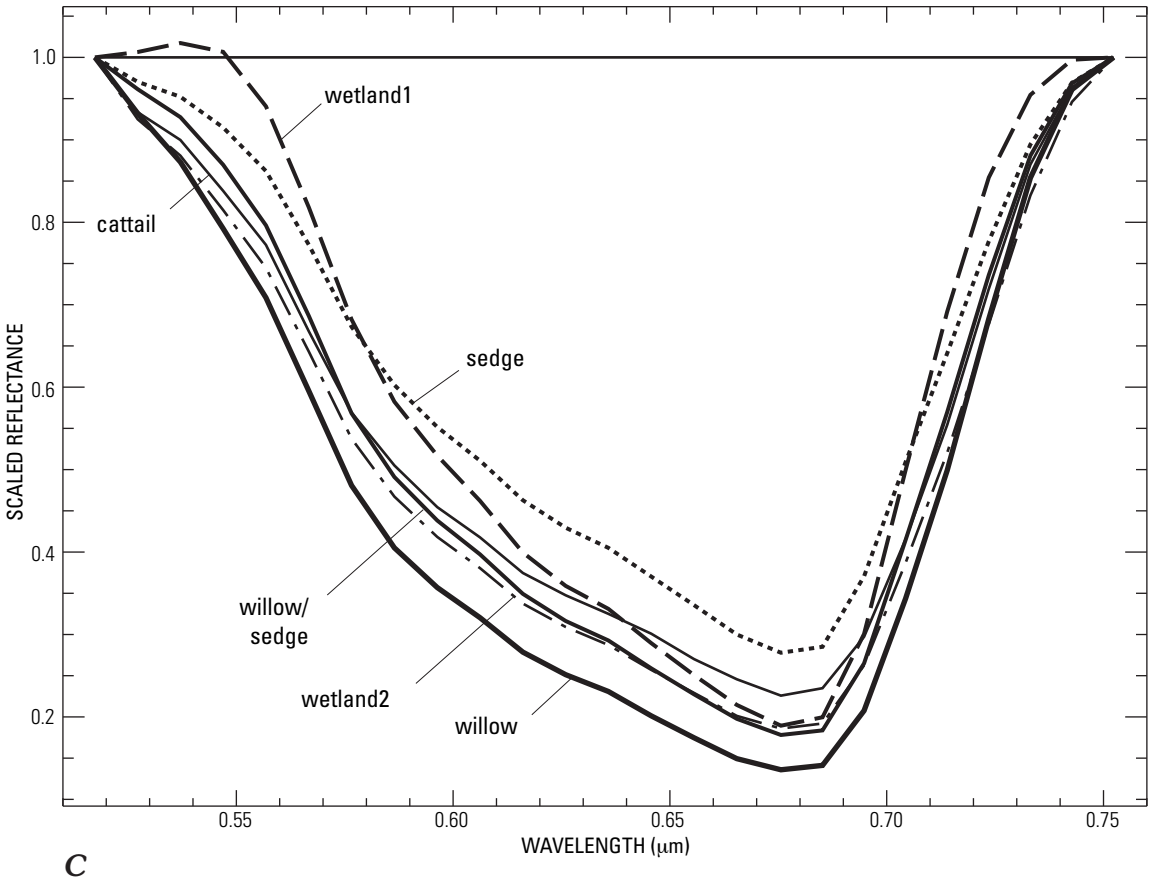
1.0
0.8
0.6
0.4
0.2
SCALED REFLECTANCE
wetland1
cattail
sedge
willow/
sedge
wetland2
willow
0.55
0.60
0.65
0.70
0.75
WAVELENGTH (μm)

C

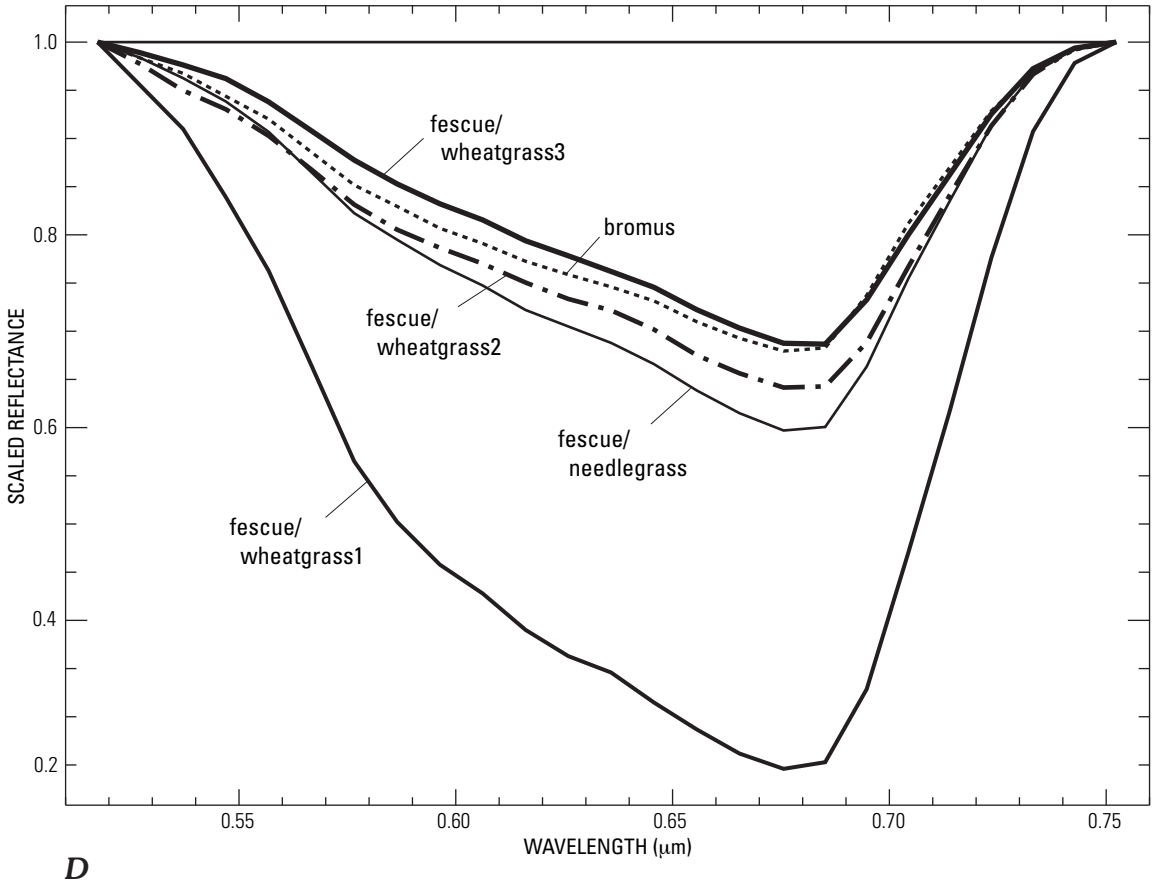
1.0
0.8
0.6
0.4
0.2
SCALED REFLECTANCE
fescue/
wheatgrass3
bromus
fescue/
wheatgrass2
fescue/
needlegrass
fescue/
wheatgrass1
0.55
0.60
0.65
0.70
0.75
WAVELENGTH (μm)

D

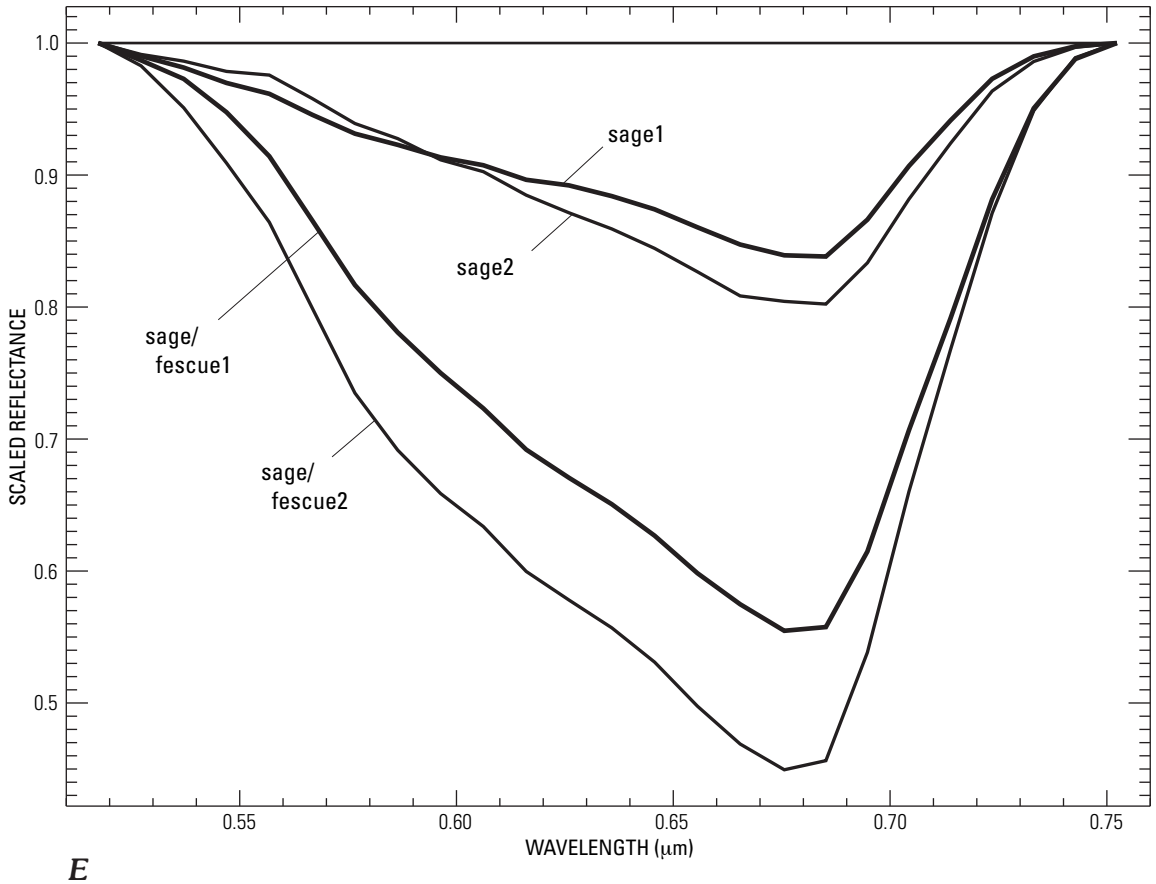

E

(SF) or Douglas fir (DF). However, the aerial-photograph analysis of Despain (1990) showed only Douglas fir in this area. Field checking revealed that, in addition to the indicated Douglas fir, there were many stands of Engelmann spruce (subalpine fir was not present). Thus, the spectral analysis was consistent in identifying the best match to these Engelmann spruce stands as being the Engelmann spruce/subalpine fir category. The map of forest cover derived from AVIRIS (fig. 8) also indicated the presence of a stand of whitebark pine (WB) in the northeast corner of the image that did not agree with the aerial-photograph interpretations. The presence of whitebark pine in these pixels was verified by field survey, and the spectral-analysis results for this area thus were confirmed.

The distributions of lodgepole pine regrowth (LP0) after the fires of 1988 also were mapped (fig. 9). During a preliminary examination of AVIRIS pixels over areas burned by the 1988 fires, we noted that some areas of LP0 cover class showed very strong chlorophyll- and water-absorption features. Consequently, the LP0 class was divided into two categories: moderate regrowth and vigorous regrowth (see the entries in table 1 and the blue and red pixels in fig. 9). When the Tetracorder results for the Mammoth Hot Springs area

Table 4. Continuum end points used for vegetation absorption features.

Cover type	Absorption feature	Left continuum range (μm)	Right continuum range (μm)
Forest			
	Chlorophyll (0.68 μm)	0.512–0.542	0.737–0.767
	Water (0.98 μm)	0.870–0.900	1.055–1.085
	Water (1.20 μm)	1.083–1.113	1.270–1.300
Nonforest			
	Chlorophyll (0.68 μm)	0.512–0.542	0.737–0.767
	Water (0.98 μm)	0.895–0.925	1.055–1.085
	Water (1.20 μm)	1.083–1.113	1.270–1.300
Bacteria			
	Chlorophyll (0.68 μm)	0.512–0.542	0.737–0.767
	Water (0.98 μm)	0.870–0.900	1.055–1.085
	Water (1.20 μm)	1.083–1.113	1.270–1.300

Table 5. Characteristics of the 0.68-µm chlorophyll-absorption feature for vegetation cover types of Yellowstone National Park.

Cover type (plot name)	Band center (µm)	Band depth	Continuum slope (μm^{-1})
	Forest		
Whitebark pine	0.6756	0.7729	0.5728
Spruce/fir	0.6756	0.7808	0.4137
Douglas fir	0.6756	0.8227	0.6714
Lodgepole pine—LP0	0.6756	0.5485	0.5103
Lodgepole pine—LP1	0.6756	0.6815	0.4300
Lodgepole pine—LP2	0.6756	0.7033	0.3744
Lodgepole pine—LP3	0.6756	0.7867	0.4747
Lodgepole pine—LP	0.6756	0.6563	0.3619
	Nonforest		
Sagebrush (sage1)	0.6852	0.1618	0.4095
Sagebrush (sage2)	0.6852	0.1978	0.4269
Sagebrush steppe (sage/fescue1)	0.6756	0.4453	0.5972
Sagebrush steppe (sage/fescue2)	0.6756	0.5506	0.6652
Grassland (fescue/wheatgrass1)	0.6756	0.7541	0.9975
Grassland (fescue/wheatgrass2)	0.6756	0.3584	0.5459
Grassland (fescue/wheatgrass3)	0.6852	0.3134	0.5933
Grassland (fescue/needlegrass)	0.6756	0.4030	0.6684
Grassland (bromus)	0.6756	0.3206	0.5222
Wet nonforest (willow/sedge)	0.6756	0.8219	1.4396
Wet nonforest (willow)	0.6756	0.8641	1.4956
Wet nonforest (sedge)	0.6756	0.7221	1.0331
Wet nonforest (cattail)	0.6756	0.7742	0.7975
Wet nonforest (wetland1)	0.6756	0.8106	1.1717
Wet nonforest (wetland2)	0.6756	0.8141	1.2318

were examined, several large areas were identified with a high concentration of vigorous lodgepole pine regrowth (indicated by red pixels in fig. 9). These areas were checked by field survey; the lodgepole pines in these areas had grown to much greater heights (more than 2 m) and densities than most of the surrounding lodgepole regrowth (≤ 1-m height). Areas of vigorous growth had high soil moisture. The higher growth rates may be related to soil moisture. The spectral differences are explained by seedling densities in the two areas. Areas of slower regrowth were a mix of grass cover and lodgepole seedlings. Areas of vigorous regrowth had an almost 100-percent cover of lodgepole pine. The spectrum of the vigorous regrowth was intermediate between that of the slower growing LP0 class and the older LP1 class.

In figures 8 and 9, a triangle-shaped patch of older lodgepole pine in the southeast corner of the AVIRIS scene was clearly indicated by the spectral analysis. The trees in this stand were interpreted to be in two age categories: 50- to 150-year-old LP1 and 150- to 300-year-old LP2. The identified age classes of lodgepole pine derived from AVIRIS data match the age classes indicated on the maps compiled from aerial-photograph interpretations; however, the spatial patterns differ. In comparing the spectra from the various areas of LP1 and LP2 age classes, overlap was observed between the spectral shapes and depths. Such a high degree of spectral similarity was not observed between other forest cover types. Consequently, it appears that additional work needs to be done to refine the age-class discriminations. Although three age classes of lodgepole pine apparently can be distinguished (LP0, LP1/LP2, and LP3), the finer discrimination of LP1 from LP2 was not always successful. This possibly is due to the fact that the two age classes do not have a clear distinguishing boundary. Indeed, the classes are age-based divisions of a continuous series. Different divisions possibly need to be developed for spectral remote-sensing data. The new age classes should correspond to observable differences in canopy spectra that result from changes in species composition, canopy structure, and percent cover of forest stands. A field study linking forest age and structure with AVIRIS canopy reflectance is needed to explore more detailed application of AVIRIS to discrimination of the ages of lodgepole stands.

The forest cover map for Mount Washburn (not pictured in this paper; see Kokaly and others, 2003) shows that most of this area is covered by lodgepole pine. However, Douglas fir (DF)

Figure 7. Continuum-removed 0.98-µm leaf-water absorption spectra. *A,* Conifer cover types. LP2, intermediate-age lodgepole pine; SF, Engleman spruce/subalpine fir; WB, whitebark; DF, Douglas fir. *B,* Lodgepole pine age classes. *C,* Lush nonforest vegetation. *D,* Grassland cover types. *E,* Sagebrush steppes.

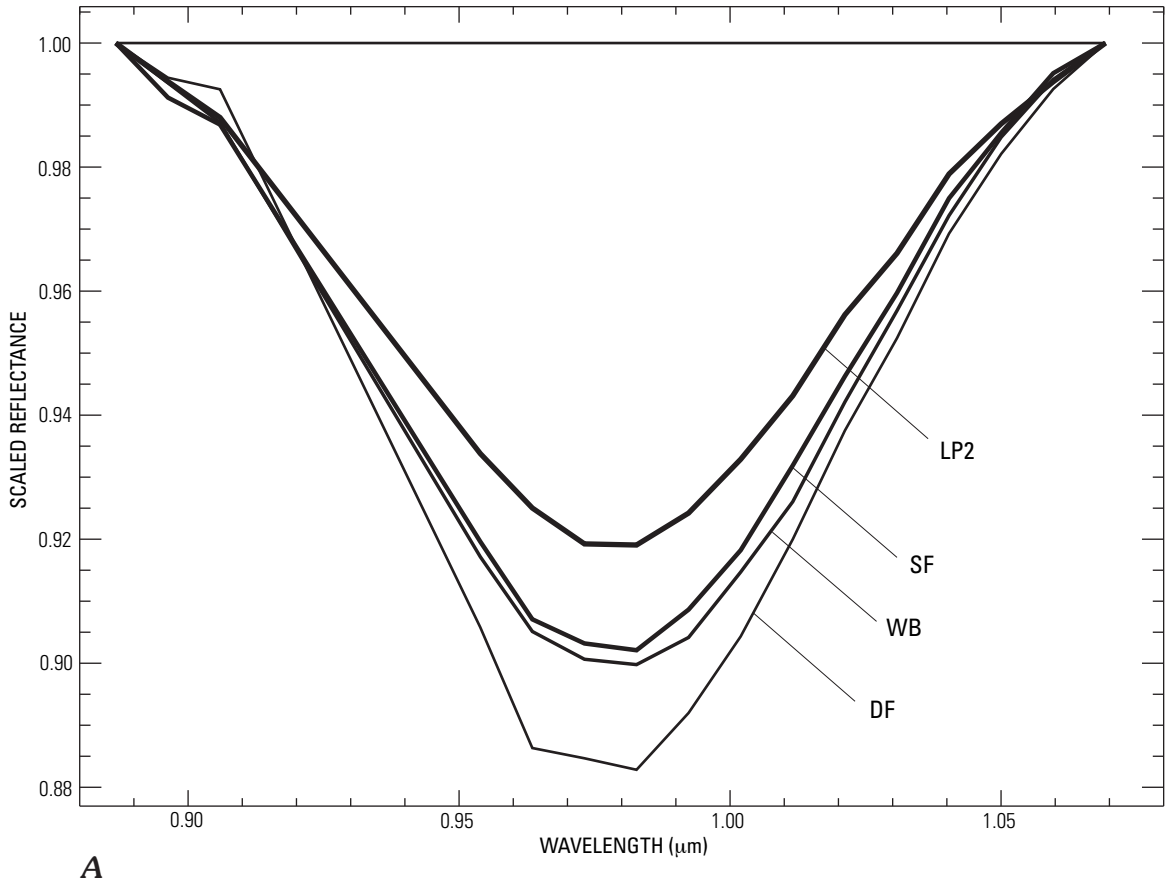
1.00
0.98
0.96
0.94
0.92
0.90
0.88
SCALED REFLECTANCE
0.90
0.95
1.00
1.05
WAVELENGTH (μm)
LP2
SF
WB
DF

A

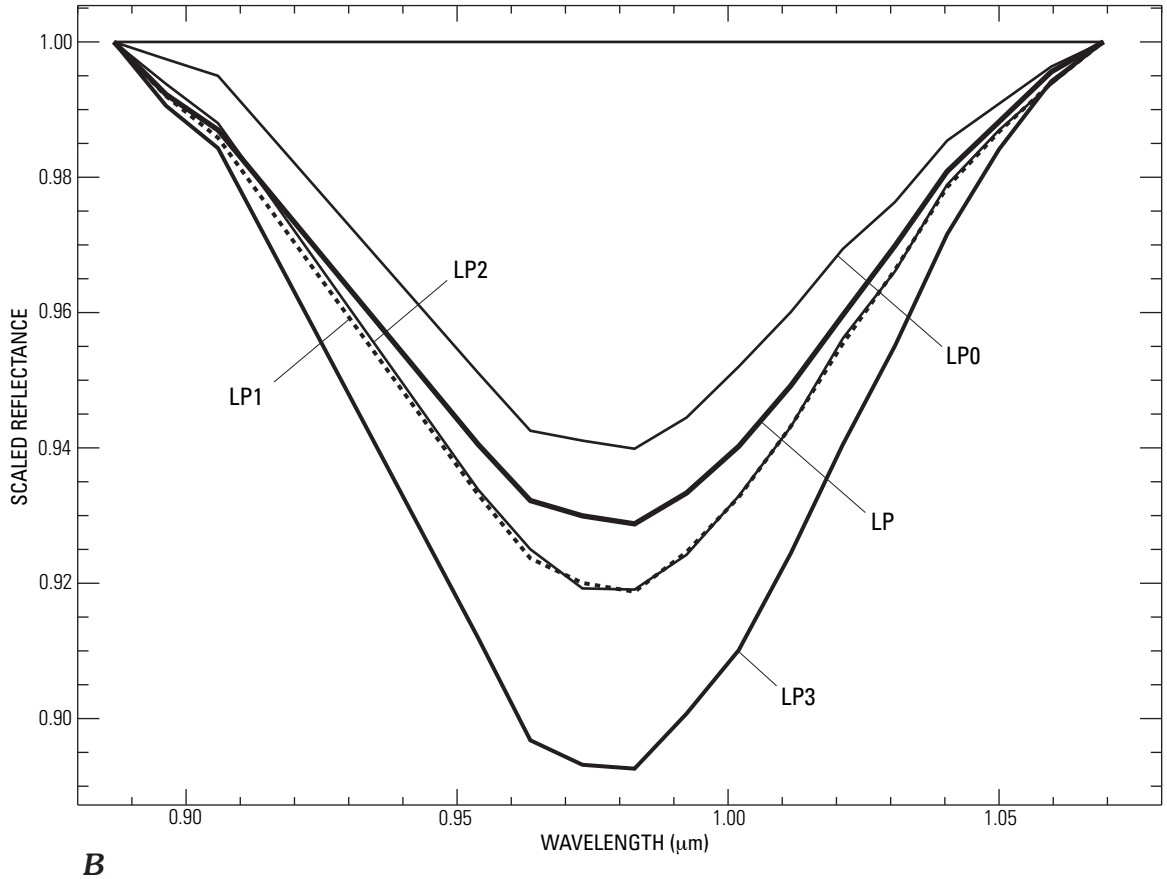
1.00
0.98
0.96
0.94
0.92
0.90
SCALED REFLECTANCE
0.90
0.95
1.00
1.05
WAVELENGTH (μm)
LP2
LP1
LP0
LP
LP3

B

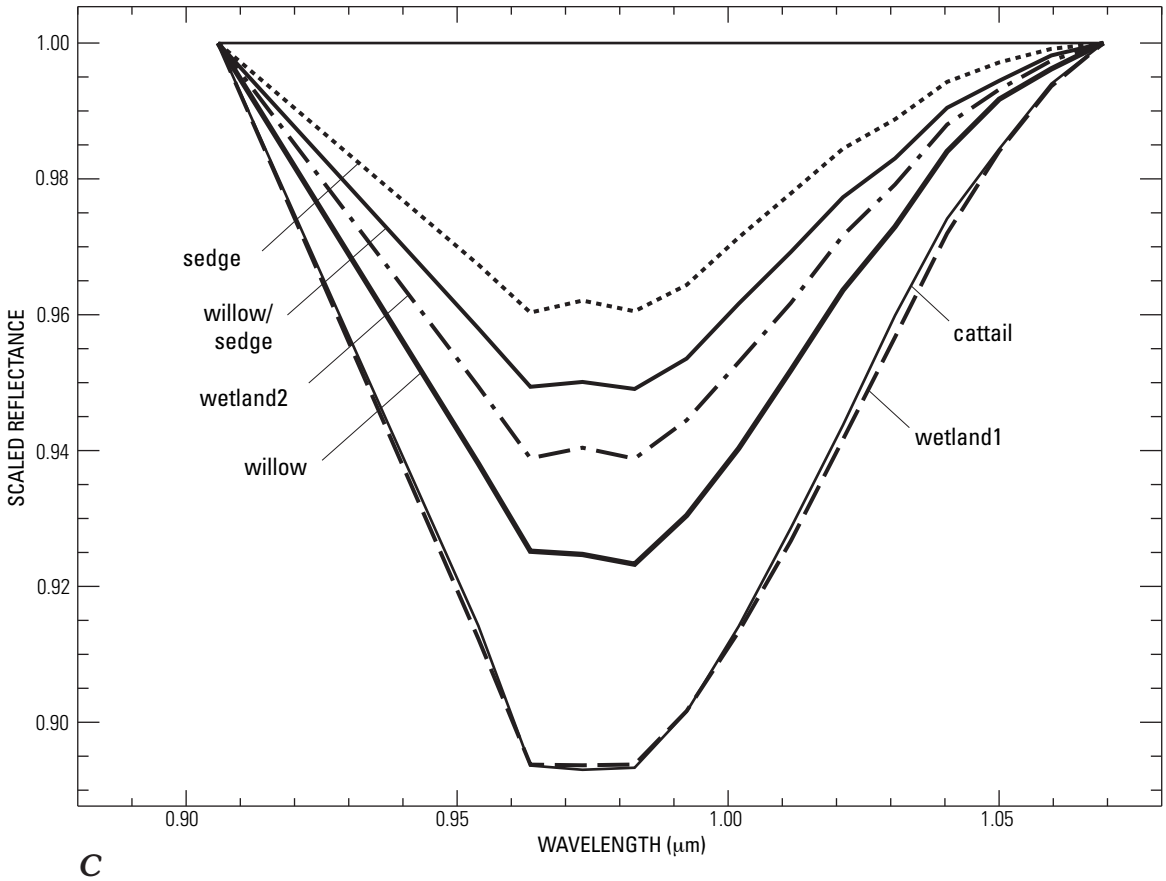
1.00
0.98
0.96
0.94
0.92
0.90
SCALED REFLECTANCE
0.90
0.95
1.00
1.05
WAVELENGTH (μm)
sedge
willow/
sedge
wetland2
willow
cattail
wetland1

C

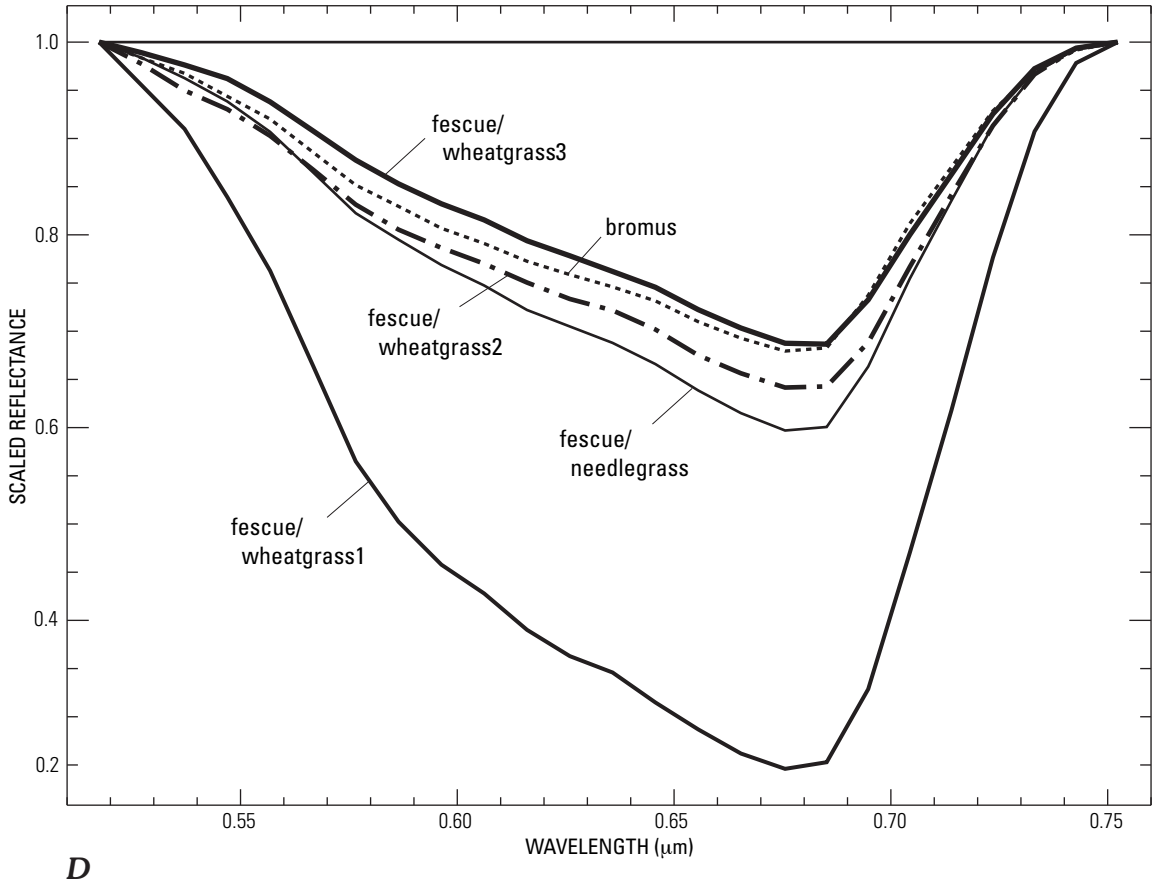
1.0
0.8
0.6
0.4
0.2
SCALED REFLECTANCE
0.55
0.60
0.65
0.70
0.75
WAVELENGTH (μm)
fescue/
wheatgrass3
bromus
fescue/
wheatgrass2
fescue/
needlegrass
fescue/
wheatgrass1

D

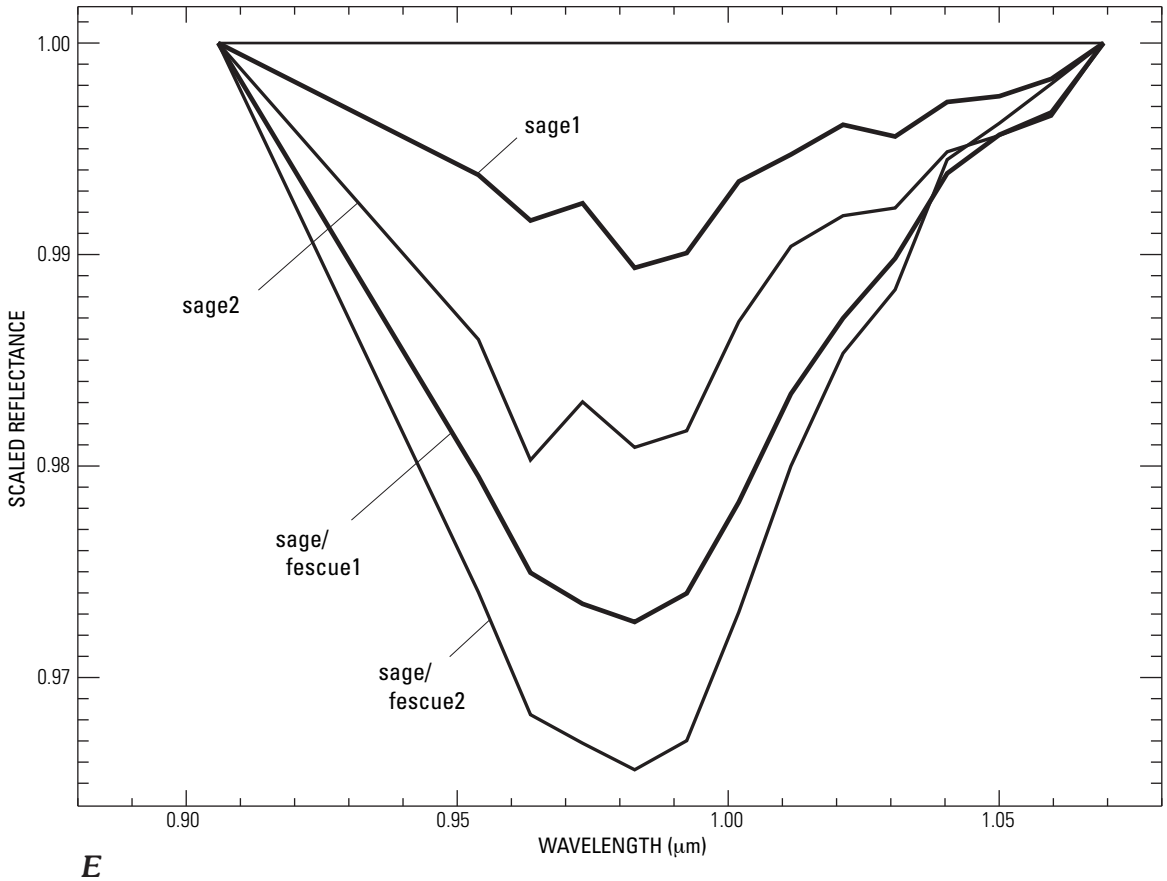

E

dominates the forest cover in the Grand Canyon of the Yellowstone River. Whitebark pine (WB) was mapped in high concentrations on the upper slopes of Mount Washburn. The mixed Engelmann spruce/subalpine fir category (SF) was present on the southern slopes of Mount Washburn at lower altitudes, and it was not present in such solid concentrations as were the other forest cover types. The high abundance of WB on the south and west slopes of Mount Washburn was confirmed by field surveys.

Overall, the distributions of forest cover types that were mapped using the Tetracorder system applied to the AVIRIS data agreed with existing maps that were compiled by Despain (1990) using aerial-photograph interpretation. Kokaly and others (2003) quantified this agreement at 74 percent (kappa statistic of 0.62). This agreement was remarkable, considering that the analytical methods of the two different types of remote-sensing data were different. In contrast to the spectral methods used here, aerial-photograph interpretation involved classification of the texture of the forest cover (including crown shapes, sizes, and shadowing). Comparison of the AVIRIS mapping results to interpreted aerial photographs revealed that the pixel-by-pixel nature of the spectral-analysis methods showed greater short-distance variation in forest cover. However, in general, the polygons drawn for different forest stands from the aerial photographs matched with the distributions derived from the AVIRIS data (compare Despain, 1990, to Kokaly and others, 2003). The distributions of whitebark pine also agreed with the expected altitude ranges of those forests; for example, whitebark pine is present at altitudes above 2,620 m (Despain, 1990). In the entire AVIRIS data set for Yellowstone National Park, whitebark pine rarely was mapped by the Tetracorder system at altitudes lower than this. The distribution of whitebark pine was confirmed in the Mount Washburn area along the trail from Dunraven Pass to the summit of Mount Washburn.

The map generated for the Mount Washburn area is used to assist in studying other parts of the Yellowstone geo-ecosystem. Whitebark pine was mapped along the slopes of Mount Washburn in areas where grizzly bears forage for food. The link between whitebark pine and grizzly bears is red squirrels, which store cones from the trees in middens; the middens are raided by grizzly bears in the fall (Mattson and others, 1992; Mattson and Reinhart, 1997). Future work in linking the AVIRIS-derived forest cover distributions with other data in a GIS analysis possibly will be useful for grizzly bear habitat delineation.

Nonforest Cover

The distributions of selected nonforest vegetation cover types for the Mammoth Hot Springs area, derived from the spectral analysis of AVIRIS data, are shown in figure 10. In this figure, the colored pixels representing the different nonforest cover types are overlaid on a gray-scale background image. Pixels that are covered by different types of vegetation or materials are depicted in gray scale. In general, white and light-gray pixels are bare ground, dark-gray pixels are forests,

Table 6. Characteristics of the 0.98-µm leaf-water-absorption feature for vegetation cover types of Yellowstone National Park.

Cover type (plot name)	Band center (µm)	Band depth	Continuum slope (μm^{-1})
	Forest		
Whitebark Pine	0.9827	0.1002	0.0658
Spruce/Fir	0.9827	0.0979	0.0765
Douglas Fir	0.9827	0.1172	0.1075
Lodgepole Pine - LP0	0.9827	0.0601	0.1430
Lodgepole Pine - LP1	0.9827	0.0813	0.1098
Lodgepole Pine - LP2	0.9827	0.0809	0.0944
Lodgepole Pine - LP3	0.9827	0.1074	0.0767
Lodgepole Pine - LP	0.9827	0.0712	0.1097
	Nonforest		
Sagebrush (sage1)	0.9827	0.0106	0.2627
Sagebrush (sage2)	0.9635	0.0197	0.1851
Sagebrush Steppe (sage/fescue1)	0.9827	0.0274	0.2238
Sagebrush Steppe (sage/fescue2)	0.9827	0.0344	0.2097
Grassland (fescue/wheatgrass1)	0.9827	0.0423	0.2418
Grassland (fescue/wheatgrass2)	0.9923	0.0093	0.2259
Grassland (fescue/wheatgrass3)	0.9923	0.0182	0.2926
Grassland (fescue/needlegrass)	0.9923	0.0221	0.2876
Grassland (bromus)	0.9923	0.0156	0.3524
Wet nonforest (willow/sedge)	0.9827	0.0509	0.1943
Wet nonforest (willow)	0.9827	0.0767	0.1586
Wet nonforest (sedge)	0.9635	0.0397	0.3195
Wet nonforest (cattail)	0.9731	0.1070	0.1518
Wet nonforest (wetland1)	0.9731	0.1063	-0.0459
Wet nonforest (wetland2)	0.9827	0.0595	0.2606

and black pixels are areas of water or deep shadows. Note that we chose not to represent all of the nonforest cover types in figure 10 in order to enhance the ability to see the depicted vegetation types in context. The other nonforest vegetation types that were identified, but not depicted, in this scene include the drier grassland vegetation types listed in table 2.

Figure 10 clearly shows where areas of sedge, willow, and wetland vegetation types are present. The riparian areas along Obsidian Creek and adjacent to Swan Lake show a mosaic pattern of dense willow stands (magenta pixels), mixed sedge and willow areas (red pixels), and areas of sedge and other wetland cover types listed in table 2 (yellow pixels). The Mammoth Hot Springs area also shows small patches of these relatively lush cover types. These patches are influenced by the geology and climate of this area. The extensive deposits of hot-spring travertine are easily penetrated by precipitation. The amount of precipitation is high in Yellowstone National Park, in part owing to the altitude of the volcanic plateaus. The precipitation likely filters through the porous travertine into depressions in the Mammoth area. The valley in which the Mammoth Hot Springs is located was shaped by glaciers that left a mosaic of depressions and mounds that concentrate water in certain areas. Similar glacial terrain on Mount Everts also is dotted with sedge and other wetland vegetation as well as small ponds. In contrast, on the rhyolitic volcanic plateau, shown in the southern two-thirds of the image in figure 10, wetland vegetation is present primarily along riparian corridors of streams.

Sagebrush shrub lands are present in two areas of the image in figure 10. Lower altitudes along the Gardner River west of Mammoth Hot Springs receive a relatively low amount of moisture compared to higher altitudes of the plateau. This climate favors growth of big sagebrush on the west slope of the Gardiner Canyon, as indicated by the results of the spectral analysis of the AVIRIS data (see blue pixels in fig. 10). At higher altitudes, near 2,194 m in the Gardner's Hole area in the vicinity of Swan Lake, the silver sagebrush cover type was mapped by the spectral analysis of the AVIRIS data (the center-left part of the image in fig. 10, also indicated by blue pixels).

Sagebrush shrub lands also were mapped in the image of the Lamar River valley (not pictured here; see Kokaly and others, 2003). At lower altitudes of the Lamar valley, pixels matched the spectra of the sage shrubland area. The higher slopes of the valley matched the areas with a higher percentage of grass relative to sagebrush (corresponding to entries of sage/fescue listed in table 1). In addition to the sagebrush cover types, much of Lamar River valley contains Idaho fescue grasslands that are mixed with

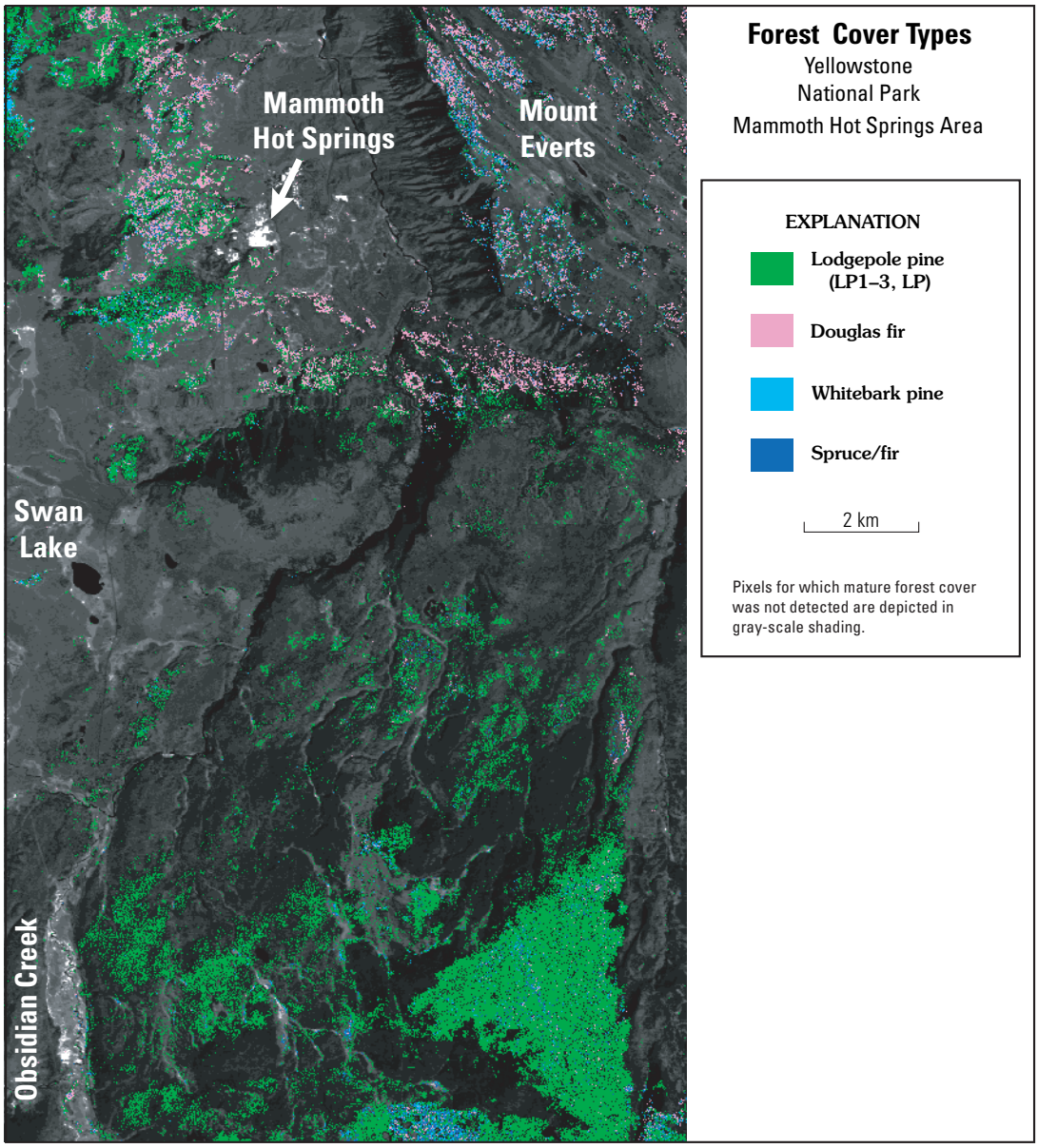

Figure 8. Map of forest cover types for the Mammoth Hot Springs area, Yellowstone National Park, derived from AVIRIS data using the USGS Tetracorder algorithm.

other grasses. Idaho fescue, Richardsons needlegrass, and bluebunch wheatgrass are mixed with the sagebrush at lower altitudes in the valley. At higher altitudes, Idaho fescue and bearded wheatgrass are prevalent. Two subcategories described by Despain (1990) of this grassland were distinguished: the drier, bearded wheatgrass phase (fescue/wheatgrass2) and the moist, sticky geranium phase (fescue/wheatgrass1). These two cover types are at higher altitudes in the scene compared to the other grasslands. These closely related cover types are near each other, but they have distinct boundaries. Possibly the undulating terrain in the valley affects the distribution of the wet phase, causing it to be present in depressions and in areas of greater snow accumulation that remain wetter throughout the year. The distribution of riparian vegetation types (willows, sedges, and wetlands) were primarily along streams and rivers, as expected. The distributions shown on the maps are reasonable, on the basis of coarse field surveys. These maps of nonforest cover types produced from AVIRIS data may be useful to assess winter-grazing resources for the large mammals in the Park, for example bison and elk. These maps, combined with other data, may contribute to a better understanding of the movements of mammal populations within and beyond Park boundaries.

Because nonforest vegetation changes drastically from season to season, the spectral signatures of the vegetation cover types derived from this specific flight do not necessarily have the same reflectance that will be recorded at different times of the year and in different years. For example, deciduous vegetation, such as willow, drops its leaves at the end of the fall and grows new ones in the spring. The number of leaves and their size and biochemical composition vary from year to year, thus altering the canopy reflectance. In addition, interannual variation in

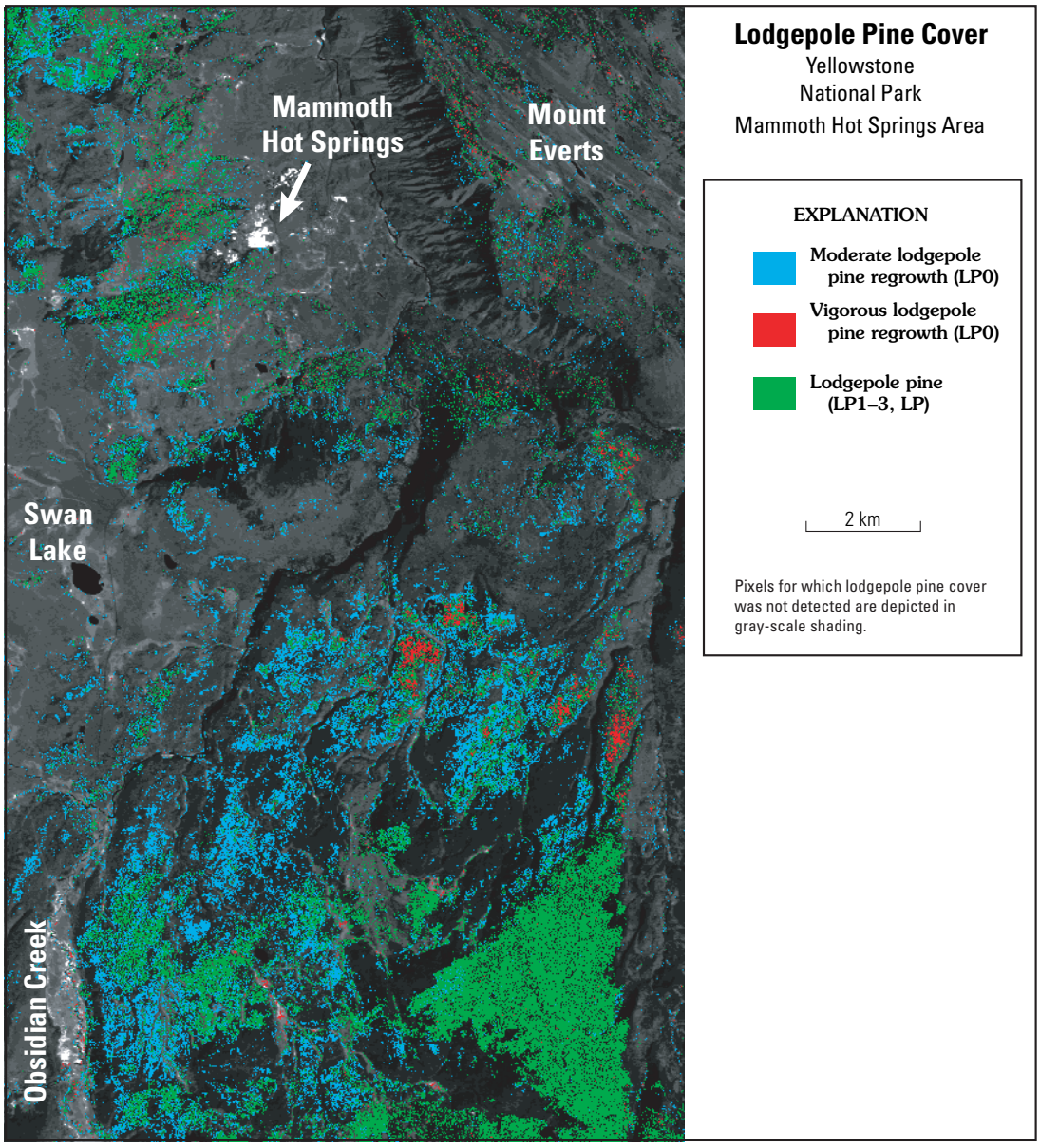

Figure 9. Map of lodgepole pine cover for the Mammoth Hot Springs area, Yellowstone National Park, derived from AVIRIS data using the USGS Tetracorder algorithm.

reflectance may result from local factors, such as precipitation or temperature, that affect the vegetation. Identification of vegetation cover types using additional AVIRIS data acquired in the future possibly will require creation of new entries in the spectral library for the nonforest areas.

The temporal changes of reflectance for evergreen conifer forests are less extreme than for other vegetation types. However, during the year, the conifers change. In the spring, reproductive bodies grow and new needles are produced (commonly a lighter shade of green). In the fall and winter, needles drop and the biochemical composition of the needles changes to produce substances that have antifreeze properties. Nonetheless, if annual flights are timed to occur at similar conditions, possibly areas derived from flights on one date will serve as a spectral library to map conifer cover types using AVIRIS data in following years.

Hot-Spring Microorganisms

The characteristic spectral signatures of hot-spring bacteria and algae in the AVIRIS remote-sensing data were used to map hot-spring microorganisms. Figure 11 shows the results for the Upper and Lower Geyser Basin areas of Yellowstone. The narrow chlorophyll-absorption and strong water-absorption features in the reflectance spectra of the hot-spring microorganisms (fig. 4) were not confused with the spectra of vegetation. For this scene, several different types of bacterial mats were used as reference entries in the spectral library that was used in the Tetracorder analysis. Most of the AVIRIS pixels that were mapped as containing hot-spring microorganisms had spectral signatures that matched a single entry in the library (see the bacteria spectrum in fig. 4). Because the conditions in which the microorganisms grow change over short lateral distances, it is likely that the 17.5-m resolution of the AVIRIS data was

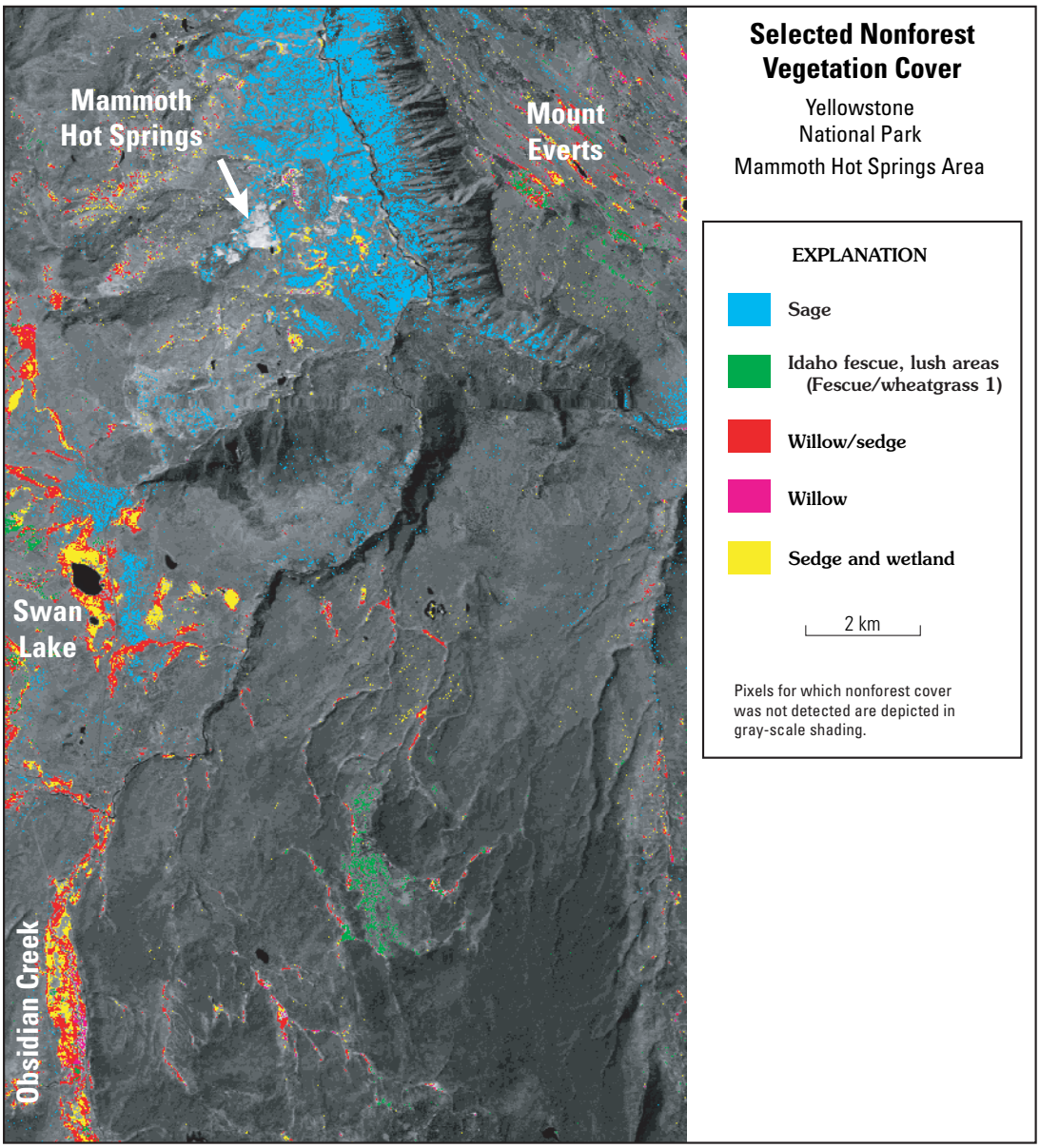

Figure 10. Map of selected nonforest cover types for the Mammoth Hot Springs area, Yellowstone National Park, derived from AVIRIS data using the USGS Tetracorder algorithm.

insufficient to resolve distinct bacterial communities. For such large pixels, each pixel potentially contains several different bacterial or algal communities, or both, in addition to surrounding vegetation and soil. Smaller pixel sizes will be more useful in identifying individual species and in defining their related environmental conditions in the hydrothermal areas.

Because each hot-spring microorganism requires specific conditions for its growing environment (for example, a narrow range of water temperature and pH; Brock, 1986), mapping the distribution of bacterial/algal mats with AVIRIS data may provide important information in the study of hydrothermal systems. Higher spatial resolution AVIRIS data (~2-m pixel size) were collected in 1998 for selected areas of the Park. These data revealed a greater diversity in reflectance signatures from microbial mats that are caused by changes in species composition (R.F. Kokaly, unpub. data). The data possibly will provide useful information for detailed study of the hot-spring bacterial and algal communities. In addition, multitemporal images could be used to study seasonal and long-term changes in the hydrothermal systems.

In Norris Geyser Basin, the maps of hot-spring microorganisms complement the information from the mineral maps made from AVIRIS (Livo and others, this volume). Maps created for both the minerals and the hot-spring microorganisms were compared. Together, these maps show the overall extent of the hydrothermal area. In some areas, the mineral signatures were weak, but the bacteria signature was very strong. Because thermophilic microorganisms live only in areas of moving hot water, we interpret those areas as having thriving microbial mats that cover the underlying material and mask the mineral signature in the reflectance spectra. Thus, use of the mineral and hot-spring-microorganisms maps in combination shows not only the overall extent of thermal areas, but also which parts had actively flowing water at the time of the AVIRIS flight.

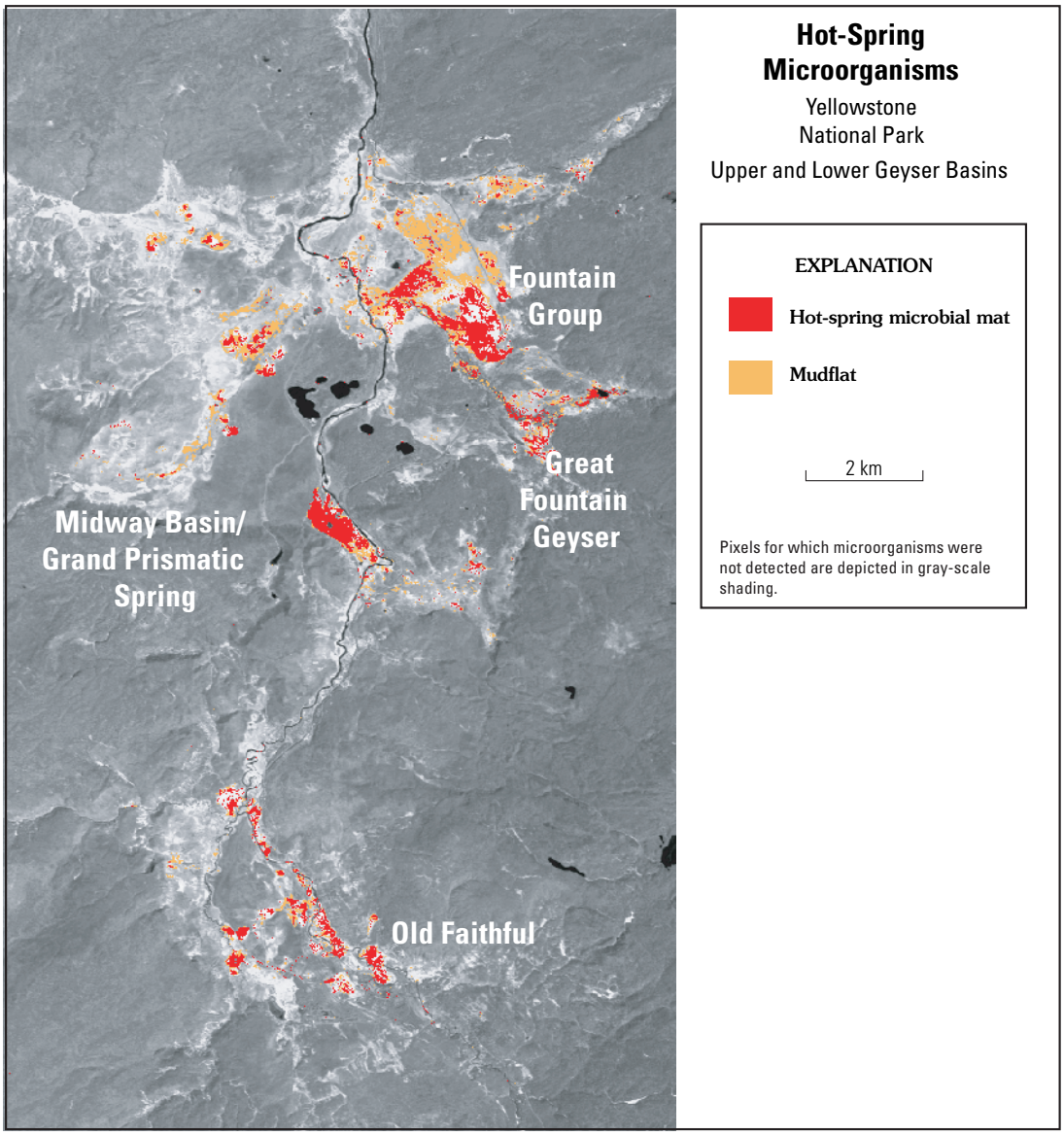

Figure 11. Map of microbial mats in the Upper and Lower Geyser Basins, Yellowstone National Park, derived from AVIRIS data using the USGS Tetracorder algorithm.

Conclusions

Airborne visible and infrared imaging spectrometer (AVIRIS) data calibrated to ground reflectance, a spectral library of vegetation reflectance, and the USGS Tetracorder system were used to produce maps of vegetation types in Yellowstone National Park. This spectroscopic approach to remote sensing included identification and mapping of forests of whitebark pine, Douglas fir, Engelmann spruce/subalpine fir, and lodgepole pine. Different age classes of lodgepole pine also were discriminated. Variations in the spectral signatures of lodgepole regrowth after the 1988 fires were observed. Representative spectra of these variations were used to differentiate and map moderate and vigorous regrowth of lodgepole pine. Nonforest vegetation types also were mapped using imaging spectroscopy, including sagebrush, wetlands, and various moisture regimes of grasslands. The chlorophyll- and water-absorption features in plant spectra were used in combination to successfully identify vegetation cover. The forest cover maps produced using Tetracorder agreed, in general, with aerial-photograph interpretations. A statistical analysis of these maps by Kokaly and others (2003) quantified the agreement at 74 percent. Field verification of vegetation cover maps also confirmed the results, including: (1) the identification of whitebark pine on the slopes of Mount Washburn, (2) mapping of Douglas fir and Engelmann spruce in the Mt. Everts area, and (3) detection of areas of vigorous lodgepole regrowth following the 1988 fires.

In this study, reflectance signatures of vegetation cover in Yellowstone National Park were created by averaging the spectra of AVIRIS pixels over known areas of vegetation. The conifers showed variation in the strengths and shapes of the pigment absorption at 0.68 μm and the leaf-water absorptions at 0.98 and 1.20 μm. The absorption strengths, as measured by

continuum-removed band depths, increased from the moderate absorption strengths in stands of lodgepole pine to the strongest absorption by Douglas fir forests. Reflectance signatures of lodgepole age classes showed variation in the near-infrared plateau region (0.7 to 1.3 μm), including increasing water absorption and decreasing continuum slope in young to middle age to old-growth stands.

Field reflectance measurements revealed a spectral signature of the hot-spring microorganisms that was distinct from the reflectance spectra of higher plants. Maps of hot-spring microorganisms were produced by comparing the field reflectance signature of bacteria to AVIRIS reflectance data. These microorganism maps complement the geologic information in mineral maps by showing areas where hot water is flowing on the surface. Future work will include efforts to discriminate and map individual species of bacteria and algae in the hydrothermal areas, in order to generate, indirectly, pH and temperature maps of hot springs. However, because bacterial and algal communities change markedly over short lateral distances, we suggest that high spatial-resolution-imaging-spectroscopy data will be even more effective for studying the hydrothermal areas.

Averaged AVIRIS spectra of vegetation canopies and field-measured-reflectance spectra of microbial mats both were compared to the spectra of AVIRIS pixels. The successful use of field spectra to map biologic materials required good calibration of AVIRIS data to surface reflectance. A combination of radiative-transfer modeling and a ground-calibration site was used. The calibrated AVIRIS data were of sufficient quality to match with laboratory measurements of minerals (Livo and others, this volume). Production of highly calibrated AVIRIS data in Yellowstone National Park in the future, during different seasons and at varying spatial resolutions, may establish the temporal consistency of canopy reflectance from conifer forest types. If the reflectance signatures of individual conifer types are consistent, the development of a set of reflectance spectra for use in mapping conifers in the northern Rocky Mountain region will be explored using the Tetracorder system and other algorithms that compare spectral shapes.

The versatility of imaging spectroscopy was demonstrated by its ability to address many issues with one data set: detection of hot-spring microorganisms, mapping of forest cover types, distinction of lodgepole pine age classes, and discrimination of nonforest vegetation types. The success of a spectral-feature-analysis approach in the remote sensing of vegetation was demonstrated. Specifically, the USGS Tetracorder system was used for normalization and comparison of spectral features. Other algorithms that focus on spectral-feature comparisons are expected to produce similar results. This analysis of AVIRIS data showed that recent advances in remote sensing, leading to the development of airborne-imaging spectrometers, have resulted in a tool applicable to the study of many parts of the Yellowstone ecosystem. In the future, additional airborne-spectrometer data should be acquired and analyzed to increase our understanding of the unique geologic features and biological systems of Yellowstone National Park.

Acknowledgments

The authors thank Ann Rodman, Ann Deutch, and the staff at Yellowstone National Park for help with research permits, field surveys, and for their enthusiastic support of our research efforts. We acknowledge Robert Green and the AVIRIS team at NASA/Jet Propulsion Laboratory for assistance in the planning and collection of AVIRIS data over Yellowstone National Park. This research was funded by the U.S. Geological Survey under the Yellowstone Project of the Mineral Resources Program.

References Cited

Adams, J.B., Smith, M.O., and Gillespie, A.R., 1993, Imaging spectroscopy—Interpretation based on spectral mixture analysis, *in* Pieters, C.M., and Englert, P.A., eds., Remote geochemical analysis—Elemental and mineralogical composition: Cambridge, Cambridge University Press, p.145–166.

Asner, G.P., and Lobell, D.B., 2000, A biogeophysical approach for automated SWIR unmixing of soils and vegetation: Remote Sensing of Environment, v. 74, p. 99–112.

Boardman, J.W., and Goetz, A.F.H., 1991, Sedimentary facies analysis using AVIRIS data—A geophysical inverse problem, *in* Green, R.O., ed., Proceedings of the third airborne visible/infrared imaging spectrometer (AVIRIS) workshop: Pasadena, NASA Jet Propulsion Laboratory Publication, v. 91-28, p. 4–14.

Brock, T.D., 1986, Thermophiles—General molecular and applied microbiology: New York, Wiley and Sons, 316 p.

Brock, T.D., 1994, Life at high temperatures—Yellowstone National Park, Wyoming: Yellowstone Association for Natural Science, History, and Education, Inc., 31 p.

Choquette, S.J., Travis, J.C., and Duewer, D.L., 1998, SRM 2035—A rare earth oxide glass for the wavelength calibration of near infrared dispersive and Fourier transform spectrometers, *in* Conference on optical diagnostic methods for inorganic transmission materials, 1998, Proceedings: Bellingham, Wash., International Society for Optical Engineering, v. 3425, p. 94–102.

Clark, R.N., 1981, Water, frost, and ice—The near-infrared spectral reflectance 0.65–2.5 μm: Journal of Geophysical Research, v. 89, p. 6,329–6,340.

Clark, R.N., 1999, Spectroscopy of rocks and minerals and principles of spectroscopy, *in* Rencz, A.N., ed., Remote sensing for the earth sciences—Manual of remote sensing (3d ed.), volume 3: New York, Wiley and Sons, p. 3–58.

Clark, R.N., Gallagher, A.J., and Swayze, G.A., 1990, Material absorption band depth mapping of imaging spectrometer data using a complete band shape least-squares fit with library reference spectra, *in* Green, R.O., ed., Proceedings of the second airborne visible/infrared imaging spectrometer (AVIRIS) workshop: Pasadena, NASA Jet Propulsion Laboratory Publication, v. 90-54, p. 176–186.

Clark, R.N., and Roush, T.L., 1984, Reflectance spectroscopy—Quantitative analysis techniques for remote sensing applications: Journal of Geophysical Research, v. 89, p. 6,329–6,340.

Clark, R.N., and Swayze, G.A., 1995, Mapping minerals, amorphous materials, environmental materials, vegetation, water, ice and snow, and other materials—The USGS Tricorder algorithm, *in* Green, R.O., ed., Summaries of the fifth annual NASA Jet Propulsion Laboratory airborne earth science workshop: Pasadena, NASA Jet Propulsion Laboratory Publication, v. 95-1, p. 39–40.

Clark, R.N., Swayze, G.A., Gallagher, A.J., Gorelick, N., and Kruse, F.A., 1991, Mapping with imaging spectrometer data using the complete band shape least-squares algorithm simultaneously fit to multiple spectral features from multiple materials, *in* Green, R.O., ed., Proceedings of the third airborne visible/infrared imaging spectrometer (AVIRIS) workshop: Pasadena, NASA Jet Propulsion Laboratory Publication, v. 91-28, p. 2–3.

Clark, R.N., Swayze, G.A., Heidebrecht, K.B., Goetz, A.F.H, and Green, R.O., 1993, Comparison of methods for calibrating AVIRIS data to ground reflectance, *in* Green, R.O., ed., Summaries of the fourth annual NASA Jet Propulsion Laboratory airborne earth science workshop: Pasadena, NASA Jet Propulsion Laboratory Publication, v. 93-26, p. 31–34.

Clark, R.N., Swayze, G.A., Livo, K.E., Kokaly, R.F., Sutley, S.J., Dalton, J.B., McDougal, R.R., and Gent, C.A., 2003, Imaging spectroscopy—Earth and planetary remote sensing with the USGS Tetracorder and expert system: Journal of Geophysical Research, v. 108 (E12), p. 5,131.

Clark, R.N., Swayze, G.A., Livo, K.E., Kokaly, R.F., King, T.V.V., Dalton, J.B., Vance, J.S., Rockwell, B.W., Hoefen, T., and McDougal, R.R., in press, Surface reflectance calibration of terrestrial imaging spectroscopy data—A tutorial using AVIRIS, *in* Green, R.O., ed., Proceedings of the 11th JPL airborne sciences workshop: Pasadena, NASA Jet Propulsion Laboratory Publication.

Despain, D.G., 1990, Yellowstone vegetation—Consequences of environment and history in a natural setting: Santa Barbara, Roberts Rinehart Publishers, 239 p.

Elvidge, D.E., 1990, Visible and near infrared reflectance characteristics of dry plant materials: Remote Sensing of Environment, v. 11, p. 1,775–1,795.

Gamon, J.A., Field, C.B., Roberts, D.A., Ustin, S.L., and Valentini, R., 1993, Functional patterns in an annual grassland during an AVIRIS overflight: Remote Sensing of Environment, v. 44, p. 239–253.

Gao, B.C., Heidebrecht, K.B., and Goetz, A.F.H., 1993, Derivation of scaled surface reflectance from AVIRIS data: Remote Sensing of Environment, v. 44, p. 165–178.

Gao, B.C., Heidebrecht, K.B., and Goetz, A.F.H., 1997, Atmosphere removal program (ATREM), Version 3.0 user's guide: Boulder, University of Colorado, Center for the Study of Earth from Space, 27 p.

Green, R.O., Eastwood, M.L., Sarture, C.M., Chrien, T.G., Aronsson, M., Chippendale, B.J., Faust, J.A., Pavri, B.E., Chovit, C.J., Solis, M., Olah, M.R., and Williams, O., 1998, Imaging spectroscopy and the airborne visible/infrared imaging spectrometer (AVIRIS): Remote Sensing of Environment, v. 65, p. 227–248.

Howard, J.A., 1991, Remote sensing of forest resources—Theory and application: New York, Chapman and Hall, 420 p.

Huete, A.F., Justice, C., and van Leeuwen, W., 1999, MODIS vegetation index (MOD 13) algorithm theoretical basis document, Version 4: NASA Goddard Space Flight Center Technical Report, available at http://eospso.gsfc.nasa.gov/atbd/modistables.html.

Ingle, J.D., 1988, Spectrochemical analysis: Engelwood Cliffs, N.J., Prentice-Hall, 590 p.

Jakubauskas, M.E., 1996, Thematic mapper characterization of lodgepole pine seral stages in Yellowstone National Park, USA: Remote Sensing of Environment, v. 56, p. 118–132.

King, T.V.V., Clark, R.N., and Swayze, G.A., 2000, Applications of imaging spectroscopy data—A case study at Summitville, Colorado, *in* Kuehn, F., King, T.V.V., Hoerig, B., and Peters, D.C., eds., Remote sensing for site characterization: New York, Springer, p. 164–185.

Kokaly, R.F., 2001, Investigating a physical basis for spectroscopic estimates of leaf nitrogen concentration: Remote Sensing of Environment, v. 75, p. 153–161.

Kokaly, R.F., and Clark, R.N., 1999, Spectroscopic determination of leaf biochemistry using band-depth analysis of absorption features and stepwise multiple linear regression: Remote Sensing of Environment, v. 67, p. 267–287.

Kokaly, R.F., Clark, R.N., and Livo, K.E., 1998, Mapping the biology and mineralogy of Yellowstone National Park using imaging spectroscopy, *in* Green, R.O., ed., Summaries of the seventh annual NASA Jet Propulsion Laboratory airborne earth science workshop: Pasadena, NASA Jet Propulsion Laboratory Publication, v. 97-21, p. 245–254.

Kokaly, R.F., Despain, D.G., Clark, R.N., and Livo, K.E., 2003, Mapping vegetation in Yellowstone National Park using spectral feature analysis of AVIRIS data: Remote Sensing of Environment, v. 84, p. 437–456.

Martin, M.E., Newman, S.D., Aber, J.D., and Congalton, R.G., 1998, Determining forest species composition using high spectral resolution remote sensing data: Remote Sensing of Environment, v. 65, p. 249–254.

Mattson, D.J., and Reinhart, D.P., 1997, Excavation of red squirrel middens by grizzly bears in the whitebark pine zone: Journal of Applied Ecology, v. 34, p. 926–940.

Mattson, D.J., Blanchard, B.M., and Knight, R.R., 1992, Yellowstone grizzly bear mortality, human habituation, and whitebark pine seed crops: Journal of Wildlife Management, v. 56, p. 432–442.

Mustard, J.F., and Pieters, C.M., 1987, Abundance and distribution of ultramafic microbreccia in Moses Rock dike—Quantitative applications of imaging spectrometer data: Journal of Geophysical Research, v. 94, p. 13,619–13,634.

Mustard, J.F., and Sunshine, J.M., 1999, Spectral analysis for earth science investigation, *in* Rencz, A.N., ed., Remote sensing for the earth sciences—Manual of remote sensing (3d ed.), volume 3: New York, Wiley and Sons, p. 251–306.

Peterson, D.L., and Hubbard, G.S., 1992, Scientific issues and potential remote sensing requirements for plant biogeochemical content: Journal of Imaging Science and Technology, v. 36, p. 445–455.

Roberts, D.A., Gardner, M., Church, R., Ustin, S., Scheer, G., and Green, R.O., 1998, Mapping chaparral in the Santa Monica Mountains using multiple endmember spectral mixture models: Remote Sensing of Environment, v. 65, p. 267–279.

Rockwell, B.W., Clark, R.N., Livo, K.E., McDougal, R.R., and Kokaly, R.F., 2002, AVIRIS data calibration information—Wasatch Mountains and Park City region, Utah: U.S. Geological Survey Open-File Report 02-199, 12 p.

Sunshine, J.M., and Pieters, C.M., 1993, Estimating modal abundance from the spectra of natural and laboratory pyroxene mixtures using the modified Gaussian model: Journal of Geophysical Research, v. 98, p. 9,075–9,087.

Sunshine, J.M., Pieters, C.M., and Pratt, S.F., 1990, Deconvolution of mineral absorption bands—An improved approach: Journal of Geophysical Research, v. 95, p. 6,955–6,966.

Swayze, G.A., Smith, K.S., Clark, R.N., Sutley, S.J., Pearson, R.M., Vance, S.J., Hageman, P.L., Briggs, P.H., Meier, A.L., Singelton, M.J., and Roth, S., 2000, Using imaging spectroscopy to map acid mine waste: Environmental Science and Technology, v. 34, p. 47–54.

Teillet, P.M., Staenz, K., and Williams, D.J., 1997, Effects of spectral, spatial, and radiometric characteristics on remote sensing vegetation indices of forested regions: Remote Sensing of Environment, v. 61, p. 139–149.

Van der Meer, F., and Bakker, W., 1997, CCSM—Cross correlogram spectral matching: International Journal of Remote Sensing, v. 18, p. 1,197–1,201.

Vane, G., Duval, J.E., and Wellman, J.B., 1993, Imaging spectroscopy of the Earth and other solar system bodies, *in* Pieters, C.M., and Englert, P.A., eds., Remote geochemical analysis—Elemental and mineralogical composition: Cambridge, Cambridge University Press, p.121–143.